Aus dem Rudolf-Virchow-Zentrum für experimentelle Biomedizin

der Universität Würzburg

Leitung: Prof. Dr. Caroline Kisker, Prof. Dr. Bernhard Nieswand

---

Role of cholesterol intermediates in supporting cell survival

Inauguraldissertation

zur Erlangung der Doktorwürde der

Medizinischen Fakultät

der

Julius-Maximilians-Universität Würzburg

vorgelegt von

Helene Nehring

aus Waldkirchen

Würzburg, April 2020

Referentin: Prof. Dr. Svenja Meierjohann

Koreferent(in): Prof. Dr. Alma Zernecke-Madsen

Dekan: Prof. Dr. Matthias Frosch

Überarbeitetes Exemplar

Tag der mündlichen Prüfung: 19.11.2020

Die Promovendin ist Zahnärztin

Table of contents

List of abbreviations .....

1 **Introduction** 1

1.1 Cell death as an essential aspect of life 1

1.2 Development of the term ‘cell death’ 2

1.3 Regulated forms of cell death 3

1.3.1 Apoptosis 3

1.3.2 Necroptosis 5

1.3.3 Pyroptosis 5

1.3.4 Parthanatos 6

1.3.5 Ferroptosis 7

1.4 Sterol regulatory element-binding proteins SREBPs 13

1.5 CRISPR/Cas9 15

1.6 Aim of the project 18

2 **Material and Methods** 19

2.1 Material 19

2.1.1 Instruments 19

2.1.2 Chemicals 20

2.1.3 Enzymes 21

2.1.4 Kits and disposables 21

2.1.5 Compounds 21

2.1.6 Antibodies 22

2.1.7 Bacteria 22

2.1.8 Oligonucleotides 23

2.1.9 Cloning vectors 24

2.1.10 Cell lines 24

2.1.11 Computer software and online tools 25

2.2 Methods 25

2.2.1 Genomic methods 25

2.2.2 Methods working with bacteria 29

2.2.3 Methods of gene transfer 29
2.2.4 Cell culture 32
2.2.5 Protein analysis 33
2.2.6 Determination of cholesterol metabolites using liquid chromatography–mass spectrometry (LC-MS) 36
2.2.7 Data presentation and statistical analyses 37
3 **Results** 38
3.1 CRISPR-based genomewide screen identified novel ferroptosis regulator 38
3.2 DHCR7 and SC5D deficiency 38
3.2.1 Sterol effect 40
3.3 Selenium impact 42
3.4 Re-expression of DHCR7 and SC5D 45
3.4.1 Pharmacological inhibition of DHCR7 48
3.4.2 Compound sensitivity 49
3.5 Impact on different cell lines 51
3.6 Genetic model of GPX4 deficiency 52
3.6.1 Impact of delipidated medium 54
4 **Discussion** 57
4.1 Antipsychotics drugs,7-DHC level and teratogenicity 58
4.2 Hepatitis B virus and 7-DHC 59
5 **Abstract** 60
6 **References** 63
List of figures 68
List of tables 68
Appendix .....
Acknowledgements .....
Curriculum vitae .....

List of abbreviations

°C	Degree celsius
µg	Microgram
µL	Microliter
µM	Micromolar
A	Ampere
AA	Arachidonic acid
ACC	Acetyl-CoA carboxylase
ACSL4	Acyl-CoA synthetase long chain family member 4
ADP	Adenosine diphosphate
Aifm	Apoptosis-inducing factor mitochondrion-associated
Akt	Protein kinase B
ALCL	Anaplastic large cell lymphoma
ALK	Anaplastic lymphoma kinase
AMP	Adenosine monophosphate
APAF	Apoptotic protease-activating factor
ARE	Antioxidant response element
ARI	Ariprazole
AT	Adenine-thymine
ATP	Adenosine trisphosphate
BAK	BCL-2 homologous antagonist
BAX	BCL-2-associated X protein
BCL	B-cell lymphoma
Bcl2a1a	B cell leukemia/lymphoma 2 related protein A1a
BFP	Blue fluorescent protein
BH	BCL-2 homology
bHLH-Zip	Basichelix-loop-helix leucine zipper
BID	BH3 interacting domain death agonist
BIM	BCL-2-interacting mediator of cell death
bp	Base pair
BSA	Bovine serum albumin
BSO	Buthionine sulfoximine
Cas	CRISPR associated
CASP	Caspase
cDNA	complementary DNA
CHX	Cycloheximide
CoA	Coenzyme A
CoQ_{10}	Coenzyme Q10
Cre	Cre recombinase
CREB	cAMP response element-binding protein
CRISPR	Clustered regularly interspaced short palindromic repeats
crRNA	Single CRISPR RNA
CTH	Cystathionine gamma-lyase
CYP51	Lanosterol 14α-demethylase

DAMPs	Damage-associated molecular patterns
DFO	Deferoxamine
DHC	Dehydrocholesterol
DHCR	Dehydrocholesterol reductase
DISC	death-inducing signaling complex
DNA	Deoxyribonucleic acid
dNTP	Deoxynucleotides
DOX	Doxorubicin
DSB	Double strand breaks
EBP	Emopamil-Binding Protein
ER	Endoplasmic reticulum/Estrogen receptor
ERA	Erastin
FA	Fatty acid
FADD	FAS-associated death domain protein
FAS	Cell surface death receptor
FASN	Fatty acid synthase
FDFT1	Squalene synthase
Fer-1	Ferrostatin-1
FIN	Ferroptosis-inducing-agent
FPP	Farnesyl pyrophosphate
g	Gravitational force
gDNA	Genomic DNA
GFP	Green fluorescence protein
GLS	Glutaminase
GPX4	Glutathione peroxidase 4
GSH	Glutathione
GSR	Glutathione-disulfide reductase
GSS	Glutathione synthetase
GSSG	Glutathione disulfide
h	Hours
HBV	Hepatitis B virus
HDR	Homology directed repair
HMGCR	HMG-CoA reductase
HMGCS	HMG-CoA synthase
HMOX	Heme oxygenase
IAP	Inhibitor of apoptosis proteins
IL	Interleukin
Indel	Insertions or deletions
INSIG	Insulin induced gene
IRES	Internal ribosomal entry site
kb	Kilo base
kDa	Kilodalton
KO	Knockout
l	Liter
LB	Lysogeny broth

LC	Liquid chromatography
LDH	lactate dehydrogenase
LDL	Low density lipoprotein
Lip-1	Liproxstatin-1
LOX	Lipoxygenase
LoxP	Locus of X-over P1
LPCAT3	Lysophosphatidylcholine acyl-transferase 3
LSS	Lanosterol synthase
M	Molar
MAM	Mitochondrial associated membrane
MAPK	Mitogen-activated protein kinase
MCL	Myeloid leukemia cell differentiation
MIF	Migration inhibitory factor
MilliQ	Ultrapure water
min	Minutes
mio	Million
ml	Milliliter
MLKL	Mixed linage kinase domain-like protein
MLV	murine leukemia virus
mM	Millimolar
MOMP	Mitochondrial outer membrane potential
MS	Mass spectroscopy
MVA	Mevalonate
MVK	Mevalonate kinase
NADPH	Nicotinamide adenine dinucleotide phosphate
Na_2SeO_3	Sodiumselenite
NCCD	Nomenclature Committee on Cell Death
NEMO	NF-κB essential modulator
NF-κB	Nuclear factor- κB
ng	Nanogram
NGS	Next-Generation Sequencing
NHEJ	Non-homologous end-joining
nm	Nanometer
nM	Nanomolar
NOS	Nitric oxide synthases
Notch	Translocation-Associated Notch Protein
NOX	NADPH-oxidases
NRF2	Nuclear factor erythroid 2-related factor 2
P	Phosphoryl group
p53	Tumor suppressor p53
PAM	Protospacer adjacent motif
PARP	Poly(ADP-ribose) polymerase
PC	Phosphatidylcholine
PCBP	Poly(rC)-binding protein
PCD	Programmed cell death

PCR	Polymerase chain reaction
PE	Phosphatidylethanolamine
PFA	Paraformaldehyde
PI	Phosphatidylinositol
PLs	Phospholipids
PLA2	Phospholipase A2
PL-OOH	Phospholipid hydroperoxides
PRR	Pattern Recognition Receptors
PUFA	Polyunsaturated fatty acid
PUMA	P53 upregulated modulator of apoptosis
PVDF	Polyvinylidene fluoride
qPCR	Quantitative PCR
RAS	Rat sarcoma
RB	Retinoblastoma
RIP or RIPK	Receptor-interacting kinase
RISC	RNA-induced silencing complex
RNA	Ribonucleic acid
ROS	Reactive oxygen species
rpm	Revolutions per minute
RT	Room termperature
SC5D	Sterol-C5-desaturase
SCAP	SREBP cleavage-activating protein
Scp2	Sterol carrier protein 2
s.d.	Standard deviation
SDH	Succinate dehydrogenase
SDS-PAGE	Sodium dodecyl sulfate polyacrylamide gel electrophoresis
Se	Selenium
sec	Seconds
Sec	Selenocysteine
sgRNA	Single guide RNA
shRNA	short hairpin RNA
SLOS	Smith-Lemli-Opitz-Syndrome
SMAC	Second mitochondrial activator of caspases
Smad	Mothers Against DPP Homolog
S2P	Site 2 protease
SQLE	Squalene monooxygenase
SQS	Squalene synthase
SRE	Sterol regulatory element
SREBP	Sterol regulatory element binding protein
Sumo	Small Ubiquitin-related Modifier
TAG	Triacylglycerid
TAK1	Transforming growth factor-β-activated kinase 1
TAM	4-Hydroxytamoxifen
Tm	Melting temperature

TM7SF2	Transmembrane 7 Superfamily Member 2
Tf	Transferrin
TfR	Transferrin receptor
TNFR	Tumor necrosis factor receptor
TNFα	Tumor necrosis factor α
α-TOH	α-Tocopherol
tracrRNA	Small trans-activation crRNA
TRADD	TNFR1-associated death domain protein
TRAF	TNFR-associated factor
TRAIL	TNF-related apoptosis-inducing ligand
TRZ	Trazodone
TXNRD1	Thioredoxin reductase 1
Ub	Ubiquitin
UV	Ultraviolet
β-Me	β-Mercaptoethanol
γ-GCS	γ-glutamylcystein synthase

1 Introduction

1.1 Cell death as an essential aspect of life

The fact that life and death belong together is beyond question. For a long time, biologists have misinterpreted cell death as “an inevitable and, hence, spurious consequence of cellular life” [2]. Decades of research have now allowed us to appreciate cell death as a necessary process involved in a wide array of biological processes. Classical examples are tissue formation during embryogenesis through the elimination of cells, tissues and organs that are transiently formed during embryonic stages. This is illustrated by the elimination of the tadpole tail during the frog development and the loss of interdigital webs of human fetus [3]. Cell death also affects the immune system through releasing damage- or pathogen-associated molecular patterns [4]. Other examples include the regulation of viral infection, wound healing and regeneration in several organisms which have also been shown to depend on cell death[5]. Moreover, the process of tumorogenesis is actively suppressed by the immune system where the recognition and triggering of cell death of transformed cells is key to this function. Unlike physiological processes, there are plenty of pathological processes and diseases where dysregulation of cell death mechanisms is associated with disease development. Mutations of proteins regulating cell survival or key oncogenic transcription factors can lead to unregulated cell growth and tumor initiation. Several neuronal diseases, autoimmunity, ischemia injuries or degenerative disorders such as Alzheimer disease have been also traced back to inappropriate cell death decisions [6], [7], [8]. Cell death is not only a cell autonomous feature as it can also impact neighboring cells. For example, dying cells can also affect the immune system through the release of damage- or pathogen-associated molecular patterns that are ultimately responsible for triggering an inflammatory response in neighboring and immune cells [4].Therefore it is beyond question that detailed knowledge about cell survival mechanisms will have a major impact on the understanding of relevant (patho)physiological processes [9].

1.2 Development of the term ‘cell death’

In 1842 Carl Vogt, a German scientist, described the process of cell death during his studies on the development of tadpoles of alytes [10]. Rudolf Virchow, the father of the cell pathology theory, described necrosis as a non-regulated and uncontrollable type of tissue destruction that leads to diseases [11]. In the midst of the 20th century the physician Glücksmann pointed out the differences between the tissue forming histogenetic cell death, the developmental biologic morphogenetic cell death and the phylogenetic cell death [12]. In 1964 Lockshin and Williams, two American scientists, coined the term of programmed cell death [13]. In the early 70s John Kerr, an Australian pathologist, coined the term apoptosis as a type of programmed cell death distinguished from necrosis [14]. In 1973 Schweichel and Merker differentiate between cell death modalities and defined three different types of cell death that are now commonly known as apoptosis, necrosis and autophagy [15]. Since then the knowledge of different types of cell death has increased and an ever-growing list of regulating factors and genes have been identified. Furthermore, there were lots of advancements and developments in methods and techniques used to characterize a biological process. An outstanding improvement of the understanding of cell death was made by Sydney Brenner in 1974. The British biologist introduced the nematode *Caenorhabditis elegans* as a model system to study cellular biology [16]. Analysis of the apoptotic pathway in *C. elegans* revealed CED-3 and CED-4 as genes involved in cell death suggesting that cell death is controlled by a genetic defined program [17]. In 1977 Chris Potten from UK released the first publication about apoptosis and reported the existence of a small group of cells in adult intestinal crypts that are extremely sensitive to apoptotic induction by irradiation [18]. In 1980 Andrew Wyllie named the relation between apoptosis and endogenous endonuclease activation. The enzyme is responsible for the cleavage of DNA, which results in characteristic DNA ladders in agarose gels. This biochemical marker is the first one proving that apoptosis was more than just an unusual morphological accident. Research during the following years showed that active mRNA and protein synthesis are necessary for the process of apoptosis. It was now asserted that apoptosis was a gene-driven mode of cell death with a biochemical mechanism distinct from that of necrosis [19], [20]. Despite the great advances in the understanding of the process of apoptosis, necrotic cell death has remained largely unexplored considering its

accidental and de-regulated nature. Today we know that there are several different types of cell death and recent insights indicate that apoptosis is neither the only form of cell death during development, nor is necrosis a completely unregulated form of cell death [21]. The Nomenclature Committee on Cell Death (NCCD) has recently composed guidelines to precisely define and interpret cell death modalities from morphological, biochemical, and functional perspectives [2].

1.3 Regulated forms of cell death

Regulated forms of cell death can either occur as an effector of physiological processes in development and tissue turnover or as an adaptive response to perturbations of the intracellular or extracellular microenvironment [22]. Regulated cell death solely occurred in physiological processes is generally equated with programmed cell death (PCD), whereby apoptosis is the most studied, and debatably the sole form of PCD. Although there is no standard consensus in the literature, it is possible to state that PCD is an essential part of evolution and that also non-apoptotic forms of PCD might exist [23].

1.3.1 Apoptosis

Apoptosis is a caspase-mediated programmed form of cell death characterized by cytoplasmic shrinkage, chromatin condensation, nuclear fragmentation and plasma membrane blebbing. Shrunk cells are often phagocytosed or split into small vesicles known as apoptotic bodies and taken up by neighboring cells. Apoptosis can be further subdivided into the extrinsic, or death receptor pathway, and the intrinsic, also known as the mitochondrial pathway [2].(**Figure 1**)

1.3.1.1 Intrinsic apoptosis

The mitochondrial-dependent pathway is triggered by different cytotoxic stimuli, such as oxidative stress, oncogenic stress, DNA damage or lack of growth factors that perturb mitochondria homeostasis [24]. Cytotoxic stimuli activate BCL-2 homology (BH3)-only motif proteins which in turn inhibit pro-survival Bcl-2 family members. Bcl-2 family members control the intrinsic pathway by regulating the pro-apoptotic multi-Bcl-2 homology (BH) domain proteins (BAX) and BH antagonist (BAK). Inhibition of Bcl-2 family members leads to activation of BAX and BAK which disrupt the mitochondrial outer membrane potential (MOMP). The increased membrane permeabilization culminates with the release of

cytochrome c from the mitochondria into the cytoplasm [2]. Cytochrome c promotes the activation of caspase 9 by combining with apoptotic protease-activating factor 1 (APAF1) and leads to activation of effector caspases and further stimulates proteolytic events [25].

1.3.1.2 Extrinsic apoptosis

The death receptor pathway is activated upon binding of death receptor ligands, such as FAS ligand TNF-α or TRAIL. Thereby a death-inducing signaling complex (DISC) is formed by the adaptor protein FADD and the procaspase-8 protein [26]. Procaspase-8 is then activated and leads to activation of truncated Bid (tBid) that interferes the mitochondrial-dependent pathway or leads to the activation of effector caspases [27].

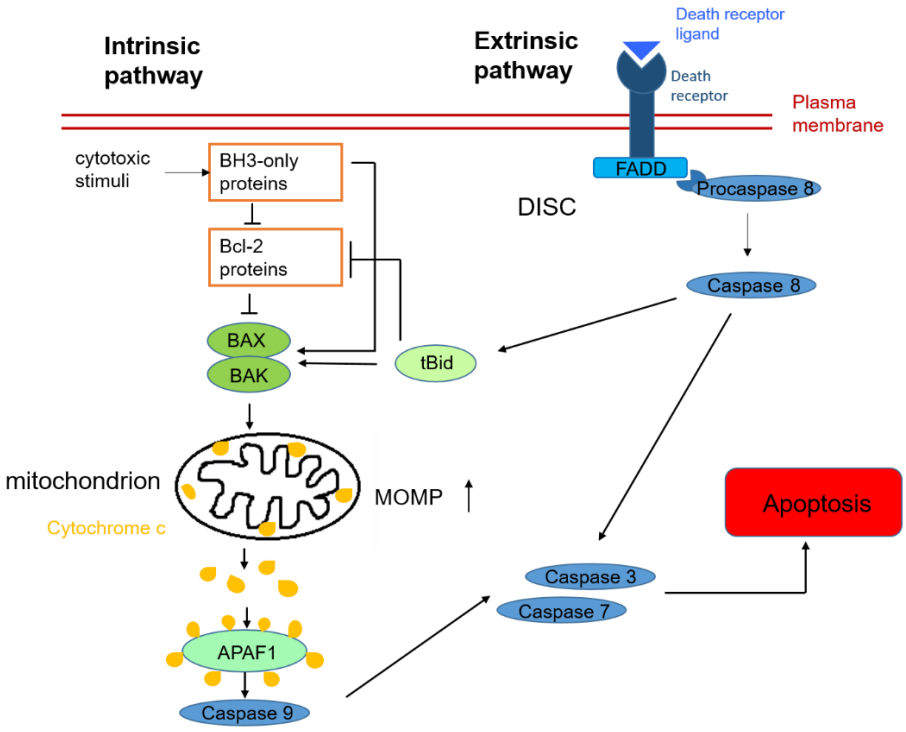

Figure 1. Intrinsic and extrinsic apoptosis signaling pathways *Apoptotic cell death can be induced by an intrinsic (mitochondrial) or extrinsic (death receptor) pathway. Both lead to the execution mechanism mediated by the effector caspases 3 and 7. Different cytotoxic stimulies can cause the intrinsic pathway by activating BH3-only proteins. BH3-only proteins inhibit anti-apoptotic Bcl2-proteins and activate pro-apoptotic BAX and BAK. That leads to mitochondrial integrity loss causing cytochrome c to be released. Cytochrome c binds APAF1 and build a complex, the apoptosome, which leads to the activation of caspase 9. Effector caspases 3 and 7 are subsequently activated by cleavage of caspase 9. Death receptor ligands, such as FAS ligand TNF-α or TRAIL initiate the extrinsic apoptotic pathway. Together with FADD and procaspase 8 they form a death-inducing signaling complex (DISC). DISC activates caspase 8 which in turn activates effector caspases 3 and 7 and leads to the activation of truncated Bid (tBid) that interfere the intrinsic pathway.*

1.3.2 Necroptosis

Necroptosis is a form of regulated cell death that is mainly induced by microenvironmental perturbations recognized by cell death receptors, such as FAS, TNFR or PRR.(**Figure 2**) It leads to a necrosis resembling morphotype characterized by oncosis, that is cell and organelar swelling followed by cell lysis and extravasation of intracellular content [2], [28]. One key element of necroptosis is the protein kinase receptor-interacting serine/threonine-protein kinase 3 (RIPK3). TNF receptor–ligand binding indirectly leads to an interaction between RIPK1 and RIPK3 and their activation [29]. The activation subsequently leads to the formation of a complex called necrosome. A key downstream factor in RIPK3-dependent necroptosis is the pseudokinase mixed-lineage kinase domain-like (MLKL) that is part of the necrosome and essential for induction of necroptosis. MLKL contains a pseudokinase domain upon RIPK3-mediated phosphorylation [30]. MLKL oligomerizes at the plasma membrane generating pore-like structures leading to permeabilization [31].

1.3.3 Pyroptosis

Pyroptosis is an inflammatory type of cell death that is dependent on the activation of either one or several caspases, such as CASP1, CASP4 or CASP5. Its morphological manifestation is characterized by a special form of chromatin condensation and cell swelling followed by plasma membrane permeabilization and osmotic lysis [32]. Specifically, CASP1 activation during pyroptosis triggers two interconnected events. First, the membrane permeabilization triggered by CASP1 is executed by gasdermin D. After cleavage of the C-terminal fragment, the N-terminal fragment of gasdermin D oligomerizes in membranes to form pores [33]. Additionally, CASP1 is a pro-inflammatory caspase and has a key role in processing of inactive IL-β and IL-18 into mature inflammatory cytokines. It is activated at complexes called inflammasomes formed after detection of bacterial toxins and viral RNA [34]. Therefore it is believed that the main function of pyroptosis is to control an infection [6].

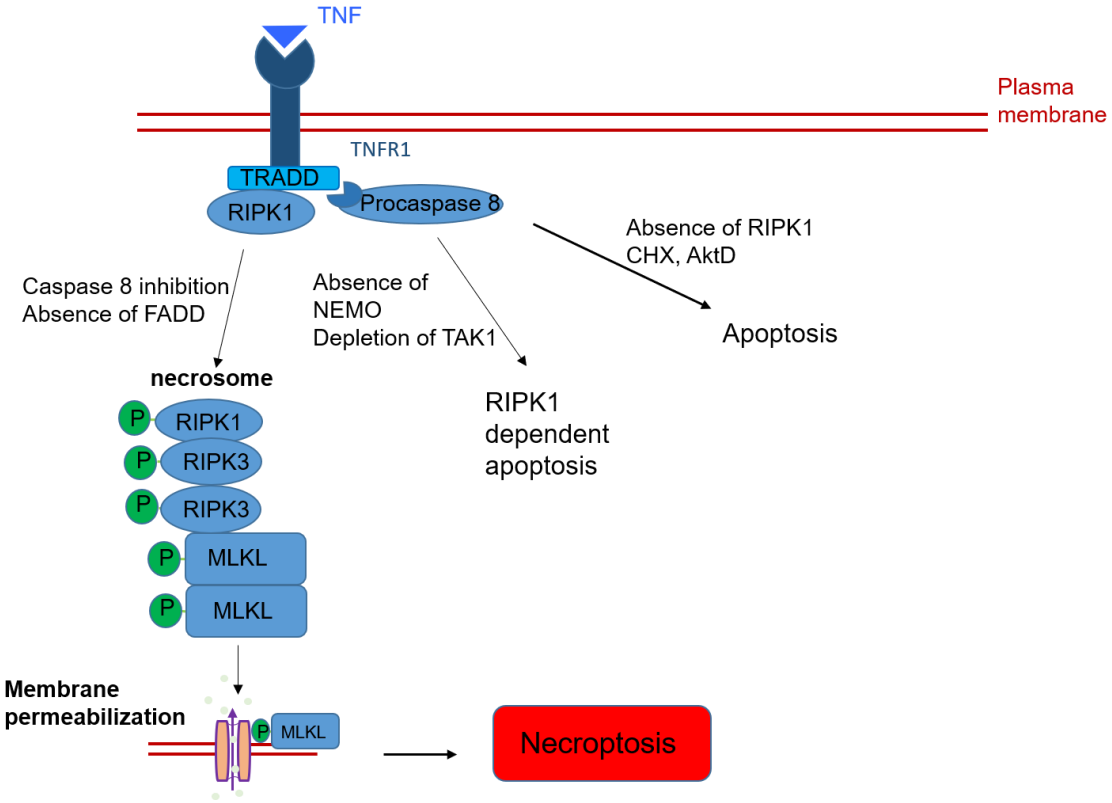

Figure 2. TNFR signaling pathways *Binding of TNFR1 ligand can initiate different pathways. By dint of TNF signals, TRADD recruits RIPK1. In the absence of active caspase 8, a microfilament-like complex called necrosome is formed by an interaction between RIPK1 and RIPK3. This interaction triggers several auto- and transphosphorylation steps that recruit and phosphorylate MLKL. Phosphorylated MLKL is translocated to the plasma membrane and permeabilize the membrane by forming pores. Integration of MLKL into the membrane causes the inflammatory phenotype of necrosis and release of DAMPs. Inhibition or depletion of TAK1 or NEMO leads to the formation of another complex and cause RIPK1 dependent apoptosis. In the presence of apoptosis inducers, such as CHX or aktD a complex with FADD is formed and caspase 8 is activated which in turn activates effector caspases 3 and 7 to execute apoptosis.*

1.3.4 Parthanatos

Parthanatos is a form of regulated cell death induced by hyperactivation of poly(ADP-ribose) polymerase 1 (PARP1) and translocation of apoptosis inducing factor mitochondria associated 1 (AIF) into the nucleus, where it leads to large-scale DNA fragmentation and chromatin condensation. The parthanatos pathway is activated in response to extensive DNA damage, oxidative stress, hypoxia, hypoglycemia, or inflammatory triggers [2]. During a screening for AIF-binding proteins the macrophage migration inhibitory factor (MIF) has been identified as a main nuclease that mediates parthanatos [35].

1.3.5 Ferroptosis

Ferroptosis is a form of regulated cell death morphologically, biochemically and genetically distinct from other forms of cell death and unique in the central involvement of iron and lipid peroxidation [36]. Besides iron metabolism, ferroptosis is connected to several biological processes, such as amino acid metabolism, synthesis of glutathione, phospholipids, polyunsaturated fatty acids, sterols and coenzyme Q_{10} (**Figure 3**). Ferroptosis is involved in different pathologies and diseases that are caused by a restricted capacity to repair peroxidized lipids [37].

1.3.5.1 Ferroptosis modulating compounds

The term Ferroptosis was coined for the first time in 2012 by Dixon et al. to describe a form of cell death induced by the small molecule Erastin. Erastin was identified in a small molecule screen campaign aiming to identify compounds that selectively kill isogenic tumor cells expressing an oncogenic mutant form of RAS. Erastin was shown to inhibit system x_c^-, a cystine-glutamate antiporter that is necessary for the biosynthesis of the antioxidant tripeptide glutathione (GSH) [37], [36]. The biosynthesis of GSH is catalyzed by glutathione synthetase (GSS) and by γ-glutamylcysteine synthetase (γ-GCS), which is the target of another, ferroptosis inducing compound, buthionine sulphoximine (BSO) [38].

In 2014 Yang et al. described RSL3 as another compound inducing ferroptosis. RSL3, unlike Erastin and BSO, was shown to directly inhibit glutathione peroxidase 4 (GPX4) without impacting GSH levels – thus underscoring GPX4 as the key enzyme translating the pro-survival function of GSH. Inhibition of GPX4 results in elevated levels of lipid reactive oxygen species and consequently cell death [37], [39]. Cells treated with Erastin or RSL3 show a different mitochondrial morphology, as mitochondria shrunk and presented a decreased membrane density and reduction of mitochondrial cristae. Erastin changes the permeability of the outer mitochondrial membrane and outer mitochondrial membrane rupture was also observed in wildtype mouse fibroblasts treated with RSL3 [40], [41]. In contrast to other forms of cell death, ferroptosis does not present nuclear or chromatin structure changes [42].

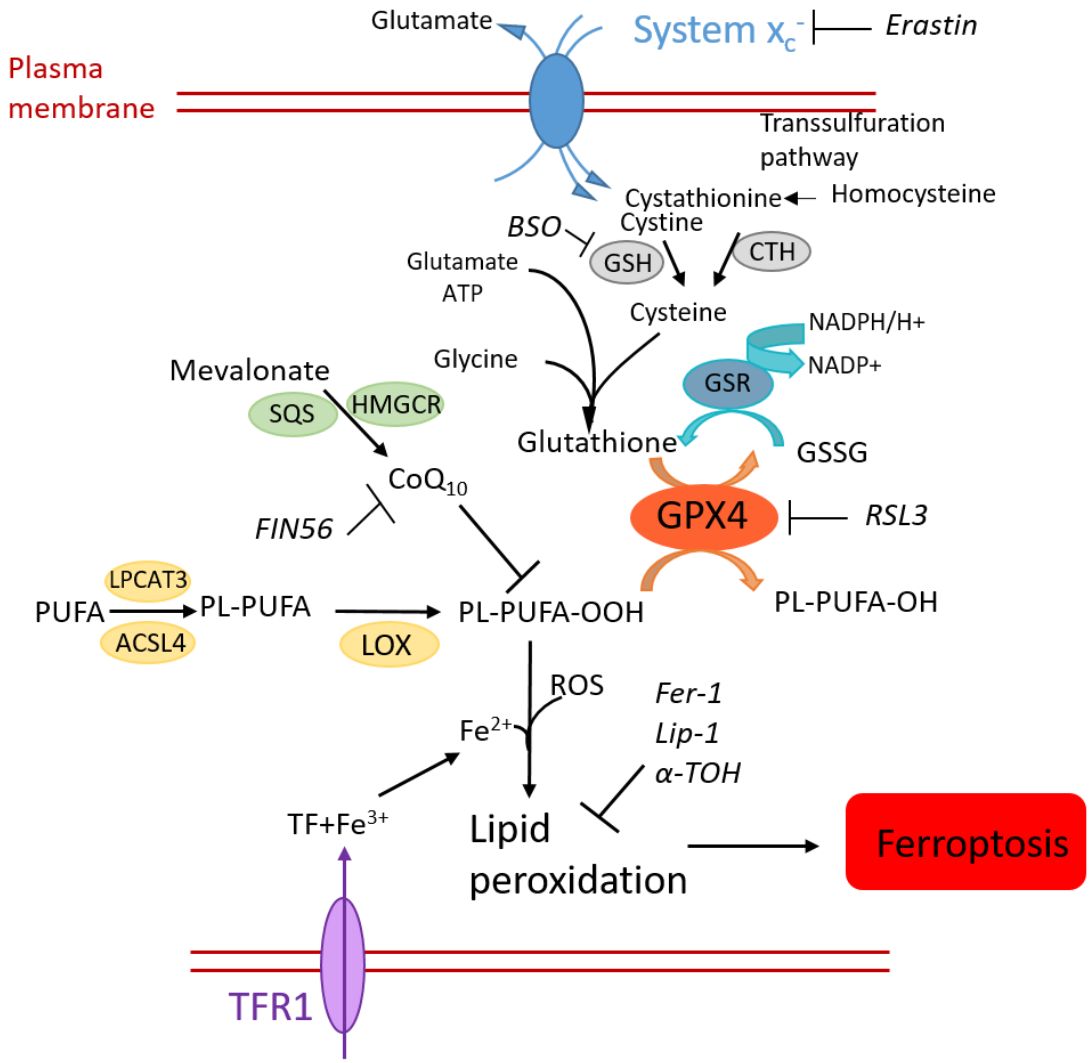

Figure 3. Ferroptosis modulating events *System x_c^- is an antiporter that imports cystine or cystathionine and exports Glutamate. Cystine is reduced to cysteine by GSH or thioredoxin reductase 1. Cysteine can also be synthesized by the transsulfuration pathway. Cysteine, as well as glutamate and glycine are required for the biosynthesis of Glutathione GSH catalyzed by γ-glutamylcysteine synthetase, γ-GCS and Glutathion synthetase, GSS. GSH is a cosubstrate for GPX4. GPX4 oxidizes two GSH molecules to GSSG and uses the electrons to reduce lipid hydroperoxides to their alcohols. Lipid hydroperoxides are substrates for iron-mediated Fenton chemistry that produces toxic lipid reactive oxygen species (ROS). Intracellular iron is stored in lysosomes after receptor mediated endocytosis of transferrin–iron complexes by the transferrin receptor 1. ACSL4 and LPCAT3 are necessary for incorporation of PUFAs in cellular membranes. LOX catalyzes the formation of lipid peroxides out of PUFAs. CoQ_{10}, a product of the mevalonate pathway, serves as an antioxidant and reduces the level of lipid peroxides. Erastin induces ferroptosis via inhibition of system x_c^- and RSL3 is a direct inhibitor of GPX4. BSO inhibits GPX4 synthesis by targeting γ-GCS. FIN56 induces ferroptosis by depleting CoQ_{10}. Fer-1, lip-1 and α-TOH inhibit ferroptosis by counteracting lipid peroxidation.*

Ferroptosis takes its name from the iron-dependency and iron chelation by deferoxamine (DFO) is able to prevent this cell death. Ferrous iron (Fe^{2+}) is catalyst of the Fenton reaction, which provides hydroxyl and peroxyl radicals intermediates that can trigger and propagate the process of lipid peroxidation. Furthermore, iron is essential for the activity of lipoxygenases (LOX), enzymes able to catalyze, in restricted contexts, ferroptosis via oxidation of polyunsaturated fatty acids (PUFAs) [43], [37]. Besides, alternative mechanisms increasing the iron-labile pool can sensitize to ferroptosis, for example the increase in iron by the degradation of heme catalyzed by heme oxygenase (HMOX). Fang et al. recently investigated causative factors involved in the pathology of doxorubicin (DOX)-induced cardiomyopathy. They revealed the activation of the nuclear factor erythroid 2-related factor 2 (Nrf2) pathway through oxidative stress as the root of HMOX1 increase and consequently cell death by iron overload and ferroptosis [44].

1.3.5.2 Lipid peroxidation

Lipid metabolism plays a key role in cellular sensitivity to ferroptosis [37]. Polyunsaturated fatty acids in phospholipids are susceptible to lipid peroxidation which can result in the induction of ferroptosis [45]. Oxygenated PUFAs can act as important signaling molecules but are also prone to decompose into reactive species with cytotoxic potential [46]. Lipid peroxidation describes the process of oxidative degradation of lipids. PUFAs can react with free radicals starting a radical chain reaction. Initially, a lipid centered radical via H-abstraction of the bis-allylic carbon. This radical intermediate subsequently reacts with diatomic oxygen to form a lipid peroxyl radical. These radicals can react with adjacent PUFA species via additional hydrogen abstraction reactions leading to the formation of lipid hydroperoxides and a new radical. Redox-active metals, such as Fe^{2+}, are then able to catalyze the generation of highly-reactive lipid alkoxyl radicals that can then re-start a new chain reaction leading to membrane damage and cell death [45]. Two enzymes, the acyl-CoA synthetase longchain family member 4 (ACSL4) and lysophosphatidylcholine acyltransferase 3 (LPCAT3) have been shown to be necessary for remodeling of PUFAs, such as acylated arachidonic acid (AA) into membrane phospholipids (PLs). Their genetic and pharmacological inhibition decreases oxidizable PUFA-PLs and hence increases resistance to ferroptosis [47]. Ferroptosis can be suppressed by ferrostatin-1 (Fer-1),

liproxstatin-1 (Lip-1) and α-tocopherol (α-Toc) whereat Fer-1 and Lip-1 have a greater potency as inhibitors than α-Toc. The ability of Fer-1 and Lip-1 to suppress ferroptosis arises rather from their activity as lipophilic radical-trapping antioxidants [48].

1.3.5.3 Mevalonate pathway

The key regulator GPX4 is not only able to reduce PUFA hydroperoxides, but also oxidized cholesterol and its esters [45]. Furthermore, increased levels of oxidized cholesterols are observed in erastin-treated cells that leads to the assumption that there is a correlation between cholesterol and ferroptosis [49]. The mevalonate (MVA) pathway is a biosynthetic pathway involved in the synthesis of sterol isoprenoids, such as cholesterol, and non-sterol isoprenoids, such as dolichol, isopentenyl-pyrophosphate and ubiquinone and is crucial for several cellular processes [50]. The active site of GPX4 consists of selenocysteine and for the efficient incorporation of selenocysteine, the selenocysteine tRNA has to be posttranscriptional modified by addition of an isopentenyl lipid group from the MVA pathway. Statins inhibit the MVA pathway, which leads to reduced GPX4 expression and increased lipid peroxidation in a subset of cells [51], [52]. Cholesterol biosynthesis is a metabolic pathway of more than thirty successive steps during which acetyl-CoA is converted to squalene, which is then further metabolized to lanosterol and other downstream sterol compounds [53] (**Figure 4**).

FIN56 is a pro-ferroptotic compound that activates squalene synthase (FDFT1), a downstream enzyme of the MVA pathway leading to cholesterol synthesis [54]. Activation of FDFT1 decreases the level of lipidated selenocysteine tRNA by depleting isopentenyl pyrophosphate that consequently reduces the availability of selenocysteine for incorporation into GPX4. Garcia-Bermudez et al discovered the loss of squalene monooxygenase (SQLE) expression, another downstream enzyme, as a cause of cholesterol auxotrophy in ALK+ anaplastic large cell lymphoma (ALCL) cell lines and primary tumors. Loss of SQLE results in accumulation of squalene, which protects ALK+ ALCL from ferroptotic cell death by preventing damage of membrane PUFAs under oxidative stress. Furthermore, genetic loss of FDFT1 inhibits squalene accumulation and resensitize SQLE-deficient cells to GPX4 inhibitors. This sensitivity of FDFT1-knockout ALCLs to GPX4 inhibitors was eliminated by adding the ferroptosis inhibitor Fer-1 or by knocking out ACSL4 and hence blocking

PUFA incorporation into phospholipids [53]. Due to activation of FDFT1 by FIN56, sensitivity to ferroptosis is enhanced. FIN56 rather causes an increase of GPX4 level but induces post-translational GPX4 degradation.

Yet another consequence of the FIN56-FDFT1 interaction is the reduced level of the upstream intermediate farnesyl pyrophosphate (FPP), which is necessary for coenzyme Q_{10} biosynthesis. CoQ_{10} is a lipophilic antioxidant and protects cells from ferroptosis. In the same manner, supplementation with FPP reduces the lethality of FIN56. Statins in turn enhance FIN56 lethality. Statins are inhibitors of HMG-CoA reductase (HMGCR), which is the first enzymatic reaction of the MVA pathway. Shimada et al. found out that idebenone, a synthetic derivative of CoQ_{10}, was the only suppressor of FIN56-induced ferroptosis but it did not affect the basal lipid ROS, contrary to α-TOH [54]. The last steps of cholesterol synthesis and intermediates and their contribution to ferroptosis need to be rationalized as an important determinant of ferroptosis sensitivity.

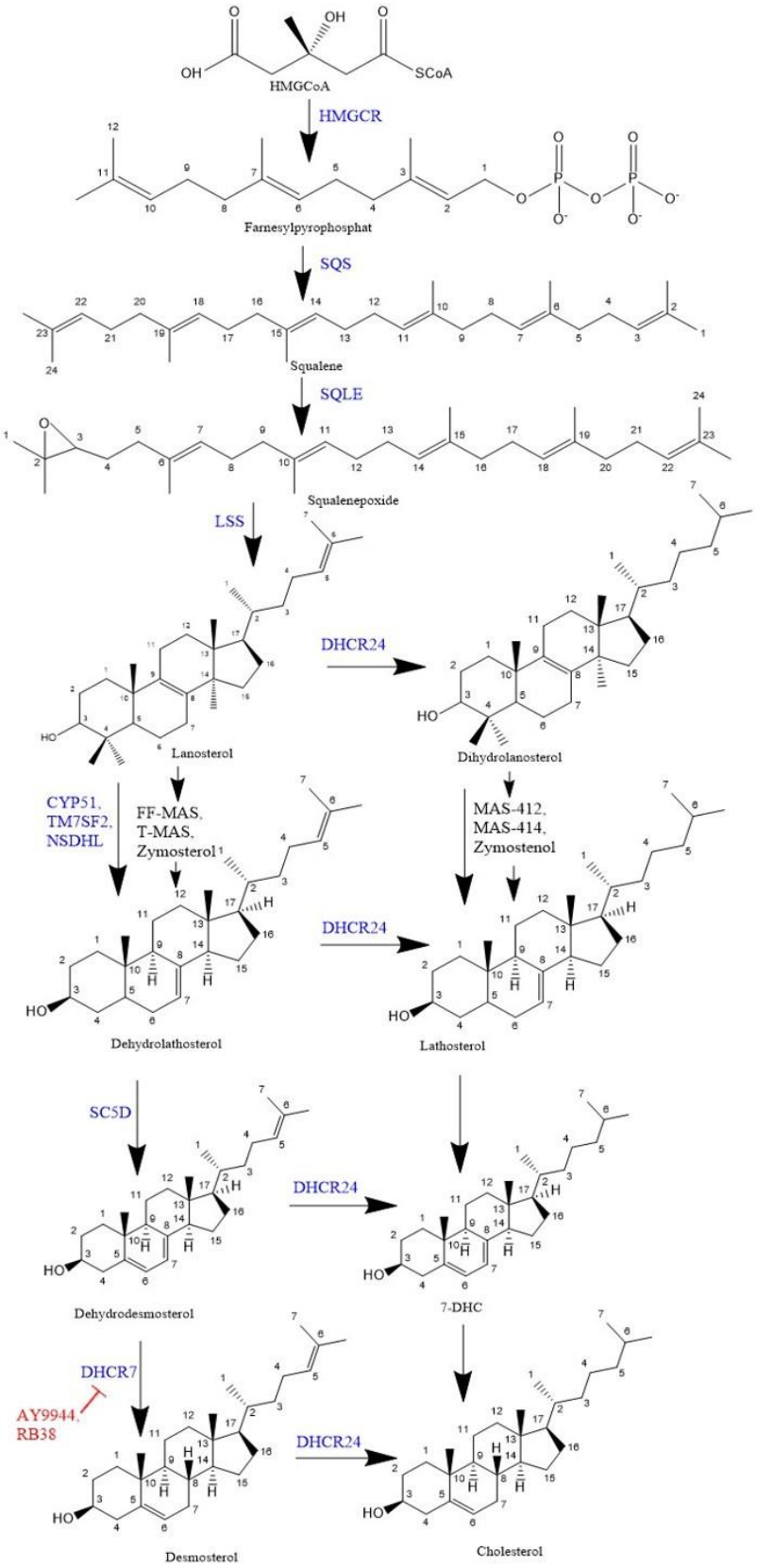

Figure 4. Cholesterol biosynthesis *Cholesterol biosynthesis is a pathway of more than thirty successive steps during which acetyl-CoA is converted to HMGCoA that is reduced to mevalonate by HMGCR. Farnesyl-PP is emerged from the mevalonate pathway and is the elementary component of squalene that is synthesized by squalene synthase (SQS). Squalene is converted to squalenepoxid by SQLE, which in turn is converted to lanosterol by LSS. Lanosterol can either be converted to dehydrolathosterol via FF-MAS, T-MAS and zymosterol or to dihydrolanosterol. Dihydrolanosterol in turn is converted to lathosterol via MAS-412, MAS-414 and zymostenol. Lathosterol is dehydrated to 7-DHC, which is hydrated to cholesterol. Dehydrolathosterol is converted to desmosterol via dehydrodesmosterol catalyzed by SC5D and DHCR7, target point for AY9944 and RB38. Desmosterol is also hydrated to cholesterol.*

1.4 Sterol regulatory element-binding proteins SREBPs

Sterol regulatory element-binding proteins (SREBPs, including SREBP1a, SREBP1c, and SREBP2) are basic helix-loop-helix leucine zipper (bHLH-Zip) transcription factors that regulate the synthesis and cellular uptake of cholesterol and fatty acids, two essential elements of cell membranes [55] (**Figure 5**). SREBPs play a critical role to support lipid homeostasis and act as important nodal points within biological signaling networks, such as regulation of anabolic metabolism during energy abundance. They are also implicated in a wide array of biological processes including endoplasmic reticulum stress, reactive oxygen species generation, inflammation, autophagy and apoptosis. Furthermore, dysfunction of this family of transcription factors has been shown to contribute to a series of human pathologies such as obesity, dyslipidaemia, diabetes mellitus, nonalcoholic fatty liver disease, nonalcoholic steatohepatitis, chronic kidney disease, neurodegenerative diseases and cancers [56]. There have been different physiological roles established for SREBPs. SREBP2 is primarily responsible for activation of genes involved in cholesterol synthesis, SREBP1c functions primarily in the liver to drive fatty acid synthesis, while SREBP1a can drive both pathways in all tissues. This strict classification has already been rebutted partly [55]. Vergnes et al. verified the function of SREBP2 in regulating cholesterol biosynthesis genes, but also revealed an unexpected role of SREBP2 in limb patterning during development and in regulating of fatty acid synthesis via compensatory upregulation of SREBP1 genes [57]. SREBPs activate expression of genes such as HMG-CoA reductase (HMGCR), HMG-CoA synthase (HMGCS), and mevalonate kinase (MVK). Moreover, they also stimulate cholesterol uptake via increased expression of the LDL receptor (LDLR) and for fatty acid synthesis, SREBPs activate expression of genes such as fatty acid synthase (FASN) and acetyl-CoA carboxylase (ACC) [55]. Trafficking between the endoplasmic reticulum, Golgi and nucleus is required for the activation and regulation of SREBPs. Mechanistically, the SREBP precursor protein is anchored in the endoplasmatic reticulum membranes, both the amino-terminal transcription factor domain and the COOH-terminal regulatory domain face the cytoplasm. Activation of SREBP is achieved by the action of SREBP cleavage-activating protein (SCAP), which forms a complex with the carboxy-terminal domains and serves as a sensor for cholesterol. At high cholesterol levels the SREBP-SCAP complex binds with

another membrane protein, insulin induced gene (INSIG), which stabilizes SREBP. Hence, at low cholesterol levels SREBP is transported to the Golgi for cleavage. The amino-terminal domain, that is still anchored in the membrane, is cleaved by another protease (site 2 protease S2P) and travels to the nucleus where it binds to sterol regulatory element-1 (SRE1) found in a myriad of genes involved in lipid homeostasis and sterol biosynthesis [58]. As lipid metabolism is a key element of ferroptosis and occurs in a variety of cancers, SREBPs provide potential targets for in-depth analysis and anti-cancer strategy aiming to trigger ferroptosis.

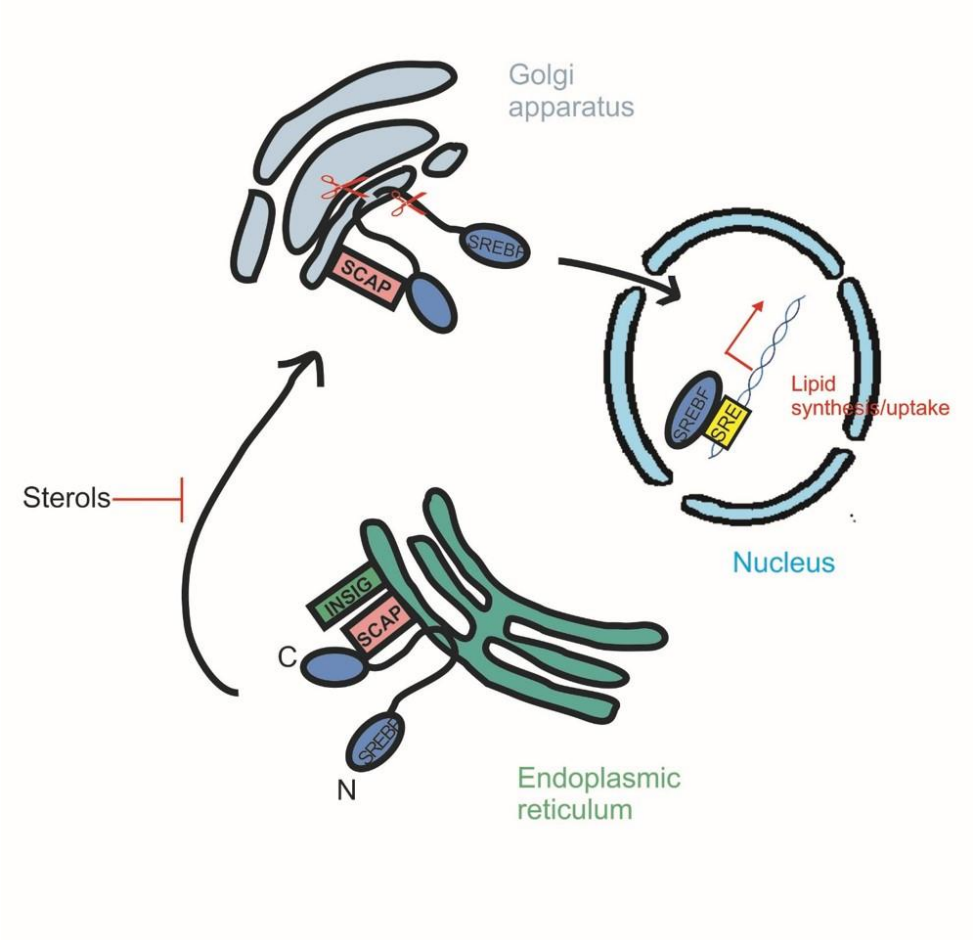

Figure 5. SREBPs regulating lipid homeostasis *At high sterol levels, the SREBP-SCAP complex is anchored in the Endoplasmic reticulum membrane stabilized by INSIG. When sterol level decreases, the SREBP-SCAP complex is transported to the Golgi apparatus to be cleaved by two proteases. The amino-terminal domain of SREBP enters the nucleus where it binds to the sterol regulatory element-1 (SRE1).*

1.5 CRISPR/Cas9

Recent advances in the field of genome engineering contributed to the discovery of an easily targetable tool for genome manipulation, the CRISPR/Cas9 technology (**Figure 6**). This method relies on an adaptive immune system in bacteria and archaea consisting of clustered regularly interspaced short palindromic repeats (CRISPR) and their CRISPR-associated sequence (CAS) proteins that provides immunization to foreign DNA of invading phages. By means of CRISPR, bacteria are able to record the invaders DNA and incorporate these spacers into a series of direct repeats of similar length. The CRISPR array includes an AT-rich leader sequence that serves as a promoter and is localized in the genome with an operon of multiple CRISPR associated proteins (Cas 1, Cas 2 and Cas 9) and a small trans-activating crRNA (tracrRNA) that regulates Cas 2 and Cas 9. After the spacer acquisition the crRNA biogenesis occurs via CRISPR transcription as a single precursor CRISPR RNA (pre-crRNA) and its following processing into mature crRNAs that each contain a single spacer. Subsequently during the interference stage, an effector complex uses the crRNA to identify and destroy any phage or plasmid whose sequence is complementary to the spacer sequence of the crRNA [59]. The spacer uptake mechanism depends on the presence of a 2-5 nucleotide pattern, the protospacer adjacent motif (PAM) [60]. Cas9 recognizes these PAM sequences in foreign DNAs and by binding a Cas1/2 complex, the selected spacer is inserted in an integrase-like reaction directly after the leader sequence of the CRISPR array [61]. The CRISPR transcription leads to a long pre-crRNA and to generate single crRNAs, the pre-crRNA is processed by RNA-specific ribonuclease III [62]. The mature crRNAs are incorporated into the effector nuclease complex consisting of Cas9 and tracrRNA. During a reinfection the effector nuclease domains recognize the recorded intruder DNA and induce local double strand breaks dependent on the presence of the PAM motif [63]. To exploit this system as a tool for genetic engineering, researchers have fused the crRNA with the tracrRNA into one single guide RNA (sgRNA) and provided new possibilities to edit DNA [64]. The induced double strand breaks are mostly repaired by non-homologous end joining (NHEJ) which leads to the generation of indels. Hence, the CRISPR/Cas9 technology enables the generation of mutations or gene knockouts by modifying the reading frame. Using two different guide

RNAs to induce two double strand breaks at different sites, a large deletion up to 20 kb can be achieved [65]. Another possibility offered by the CRISPR/Cas9 technology is a precise gene replacement by using homology directed repair (HDR). Therefor a DNA repair template containing the desired sequence is delivered into the cell and facilitates changes ranging from a single nucleotide change to large insertions with high specificity [66].

CRISPR has also boosted the potential of large-scale forward genetic screening by using pooled lentiviral CRISPR libraries. Pooled lentiviral CRISPR libraries are a heterogenous population of lentiviral transfer vectors, each containing an individual gRNA targeting a single gene in a given genome. The gRNAs identified in the screen can be tested to ensure that they reproduce the phenotype of interest [67]. In the context of ferroptosis it is essential to mention that a first generation CRISPR-based genetic screen uncovered ACSL4, demonstrating its proferroptotic role [36]. Recently, significant improvements in the CRISPR system and development of a second-generation gRNA library allow for higher knockout efficiency and markedly reduced off-target effects [68]. In the present work we followed to characterize one hit originating from a second generation CRISPR screen and provide evidence for a new player in the ferroptosis network.

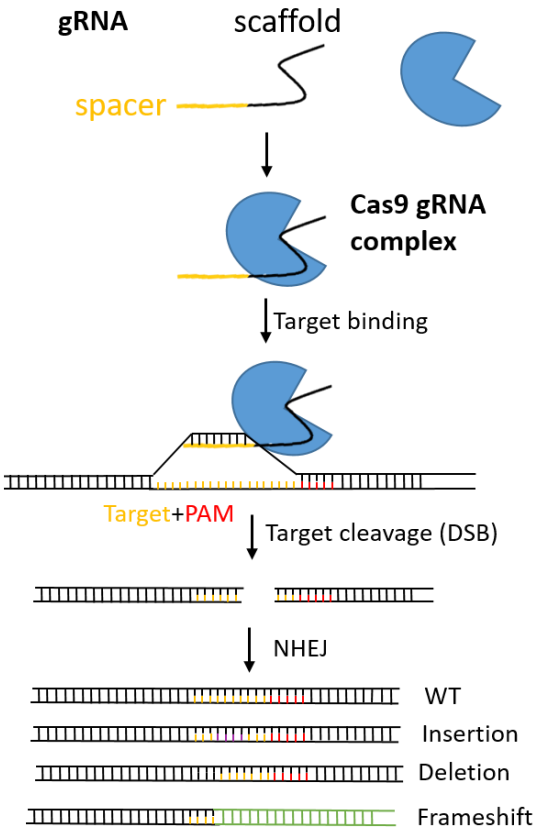

Figure 6. CRISPR Cas9 system *The gRNA combines with Cas9 that leads to the formation of a Cas9 gRNA complex. The PAM sequence serves as a binding signal for Cas9 and the spacer region of the gRNA interact with target DNA. If the spacer sequence is homologous to the target DNA Cas9 induces a DNA cleavage that leads to a double-strand break within the target DNA about 3-4 nucleotides upstream of the PAM sequence. The DSB is then repaired by the most active non-homologous end joining pathway that causes indels in the target DNA that result in amino acid deletions, insertions, or frameshift mutations.*

1.6 Aim of the project

Based on the depicted level of knowledge, the aim of this project is to study the role of cholesterol intermediates in supporting cell survival. Using the CRISPR/Cas9 system, knockouts of DHCR7 and SC5D, two upstream regulating enzymes of cholesterol biosynthesis, were generated in HT1080 cells. These cell lines are utilized to validate the impact of these enzyme functions and their substrates lathosterol and 7-dehydrocholesterol on cell viability. In this thesis, we will examine to what extent DHCR7 and SC5D deficiency affects the cellular sterol composition, the sensitivity to cell death inducing compounds and whether expression of ferroptosis regulating enzymes is altered. Besides the DHCR7/SC5D KO cell lines, we generated cell lines that re-express the enzymes to validate the enzyme activity more particularly. Furthermore, the role of selenium concerning its essential function in selenoproteins and the correlation between cell medium content of selenium and cell viability will be investigated. Besides selenium, it will be clarified to what extent the medium content of sterols affects the behavior of our cell lines and the impact of cholesterol intermediates on different cell lines will be illustrated. Next, the role of sterols will be examined in a genetical model of ferroptosis by using the genetical tool CreER/loxP system. In general, this thesis will elucidate the meaning of cholesterol intermediates for diseases and incites for in-depth research on this topic.

2 Material and Methods

2.1 Material

2.1.1 Instruments

Instrument	Company
c400 Visible Fluorescent Western System	Azure biosystems
Thermo Scientific™ Safe 2020	Thermo Fisher Scientific
Microscope AE31E	Motic
Thermocycler peqSTAR	VWR
C150 CO2 Incubator	Binder
Centrifuge 5417c	Eppendorf
Power supply	Major Science
Spark® Multimode Microplate Reader	Tecan
PerfectBlue™ Horizontal Minigelsystems	PEQLAB Biotechnologie
Cast-It™ Gel CASTER	PEQLAB Biotechnologie
PerfectBlue™ 'Semi-Dry' Electro Blotter	PEQLAB
Mr. Frosty™ freezing container	Thermo Fisher
Nanophotometer	Implen
Neubauer counting chamber	Paul Marienfeld GmbH
New Brunswick™ Excella E24 Incubator shaker	Eppendorf
Roller shaker RS TR5	Phoenix
Microwave	Severin
Lourmat TFX-35	Vilber
Sonification device Q125	Qsonica
SpectraMax M5 Microplate Reader	Molecular Devices
Thermal Shake Lite	VWR
Vortex TX4	VELP scientific
Waterbath VWB 12	VWR
Precision Balance	VWR
Thermo Scientific Heraeus Function Line Incubator	Thermo Fisher Scientific
Dionex Ultimate 3000 UHPLC Sytem	Thermo Fisher Scientific
Liquid Nitrogen LS600	Worthington Industries
Filtropur V50 0.45, Vacuum Filter	Sarstedt

2.1.2 Chemicals

Chemical	Company	Cataloge no
Acrylamide	Carl Roth	A124.2
Ammonium persulfate	Carl Roth	9178.3
Ampicillin	Carl Roth	K029.2
Blasticidin	InvivoGen	Ant-bl-05
Bromophenol Blue sodium	AppliChem	A3640,0005
BSA, fatty acid free	Roche	10775835001
DMSO	Carl Roth	A994.1
dNTP Mix	Biozym	331520
DNA Agarose	Biozym	840004
DNA loading Dye 6x	Thermo Fisher	R0611
EDTA	Carl Roth	8040.2
Ethanol (EtOH)	Merck	1009831000
Fetal Bovine Serum	Corning	35079-CV
Hydrochloric Acid (HCl)	Sigma-Aldrich	H1758
Isopropanol	Applichem	0001384874
Magnesium sulfate (MgSO4)	Carl Roth	0261.1
Methanol	AppliChem	0001264766
Midori Green	Nippon genetics	461MG15088
Panexin	PAN biotech	P04-96090
Penicillin-Streptomycin	Lonza	17-602E
Powdered milk	Carl Roth	T145.3
Protamine sulfate salt from salmon	Sigma-Aldrich	P4020
Puromycin	InvivoGen	ant-pr-1
Silica	Sigma-Aldrich	S5130
Sodium Dodecyl Sulfate (SDS)	AppliChem	L3771-1KG
Sodium Hydroxide (NaOH) 98%	Roth Carl	PO31.2
Sodium Phosphate	Sigma-Aldrich	342483-25G
Temed	Carl Roth	2367.1
Tris	Carl Roth	2449.3
Triton X	Sigma-Aldrich	93443
Tris hydrochloride	Carl Roth	90903
Tween 20	Sigma-Aldrich	P9416
X-TremeGene™ HP DNA Transfection Reagent	Roche	6366236001
β-Mercaptoethanol (ß-Me)	Roth Carl	4227.3

2.1.3 Enzymes

Enzyme	Company	Cataloge no
DreamTaq Green PCR Master Mix	Thermo Fisher	K1082
Proteinase K	Roth Carl	7528.1
Restriction Endonucleases (BbSI HF, BstBI, XhoI)	New England Biolabs	various
T4 DNA Ligase	New England Biolabs	M0202S
Q5® High-Fidelity DNA Polymerase	New England Biolabs	M0491L
Phusion™ High-Fidelity DNA Polymerase	Thermo Fisher	F-530XL
NEBuilder® HiFi DNA Assembly Master Mix	New England Biolabs	E2621L

2.1.4 Kits and disposables

Kit/disposable	Company	Cataloge no
0.05 % Trypsin-EDTA (1x)	Life Technologies	25300054
Resazurin sodium salt	Sigma-Aldrich	R7017
BCA Protein Assay Kit	Thermo Fisher	23227
cOmplete™ ULTRA Tablets (Protease Inhibitor Cocktail)	Roche	5892988001
Dubeccos Modified Eagle Medium (DMEM)	Life Technologies	21969035
Dubeccos Phosphate Buffered Saline (DPBS)	Life Technologies	14190094
Wizard® SV Gel and PCR Clean-Up System	Promega	A9282
Monarch Plasmid Miniprep Kit	New England Biolabs	T1010L
Nunc® CryoTubes®	Thermo Fisher	V7634-500EA
Page Ruler Plus	Thermo Fisher	00691792
Pierce™ BCA Protein Assay Kit	Thermo Fisher	23225
Plasmid Maxi Kit	Qiagen	12163
SOC Outgrowth Medium	New England Biolabs	B9020S
WesternBright ECL HRP substrate	Advansta	K-12045-D50

2.1.5 Compounds

Compound	Company	Cataloge no
AY9944	Cayman Chemical	14611
Auranofin	Sigma-Aldrich	A6733
Bortezomib	Sigma-Aldrich	5.04314

Carfilzomib	Sigma-Aldrich	791938
Cholesterol	Sigma-Aldrich	C8667
Erastin	Selleckchem	S7242
FIN56	Sigma-Aldrich	SML1740
Lanosterol	Cayman Chemical	19521
Lathosterol	Sigma-Aldrich	700069P
Liproxstatin 1	Sigma-Aldrich	SML1414
Luperox® TBH70X, tert-Butyl hydroperoxide solution	Sigma-Aldrich	458139
ML210	Sigma-Aldrich	SML0521
Tamoxifen	Selleckchem	S7827
Tasin 1	Sigma-Aldrich	SML 1988-5MG
7-Dehydrocholesterol	Sigma-Aldrich	30800-5G-F

RB38 was a kind gift from Prof. Dr. Peter Imming (Halle) and RSL3 was a kind gift of Derek Pratt (Canada).

2.1.6 Antibodies

Antibody	Company	Cataloge no
Anti-mouse IgG	Cell Signaling Technology	7076S
Anti-rabbit IgG	Cell Signaling Technology	7074S
Anti-rat IgG	Cell Signaling Technology	7077S
Rabbit Anti-Glutathione Peroxidase 4 antibody	abcam	ab125066
Rabbit Anti-Glutathione Peroxidase 1 antibody	Cell signaling Technology	3286S
Mouse Monoclonal Anti-Flag M2 antibody	Sigma-Aldrich	F3165-2MG
B-actin	Sigma-Aldrich	A5441
ACSL4	Santa Cruz Biotechnology	Sc-271800

AIFM2 and Thioredoxin Reductase 2 are self-made antibodies of the Helmholtz antibody facility.

2.1.7 Bacteria

Dh5α competent *E. coli*

2.1.8 Oligonucleotides

2.1.8.1 Genotyping

Oligo label	Sequence (5‘-3‘)
hDCHR7_Fw1	TGAAGCAAGTTCCATCCCC
hDCHR7_Rev2	ACCCCCTTCAAAACCCACAG

2.1.8.2 Cloning

Oligo label	Sequence (5‘-3‘)
p442-Gb-ER-TM_Fwd	CCGGTCGAATCAAGCTTATCGATACCGTCGA CGGATCCTTATGGGTGCTTCAGGAGAC
p442-Gb-SREBP1a	ATTGCTCGGAGGGCCCCGGGCGGCCGCTACG TAACCGGTCCTAGTCAGGCTCCGAGTCACTG CCACTGCCACC
p442-Gb-SREBP2	ATTGCTCGGAGGGCCCCGGGCGGCCGCTACG TAACCGGTCCTAGTCTGGCTCATCTTTGAC

2.1.8.3 Sequencing

Oligo label	Sequence (5‘-3‘)
pKLV_U6_sequencing2	TTCACCGAGGGCCTATTTCCCATG
pIRES-RP	TATAGACAAACGCACACCG
p442_seq_for	CCGAGCTCTATAAAAGAGCTCACAACC
p442_seq_REV	ATCGGGCTGCAGGAATTGCT

2.1.9 Cloning vectors

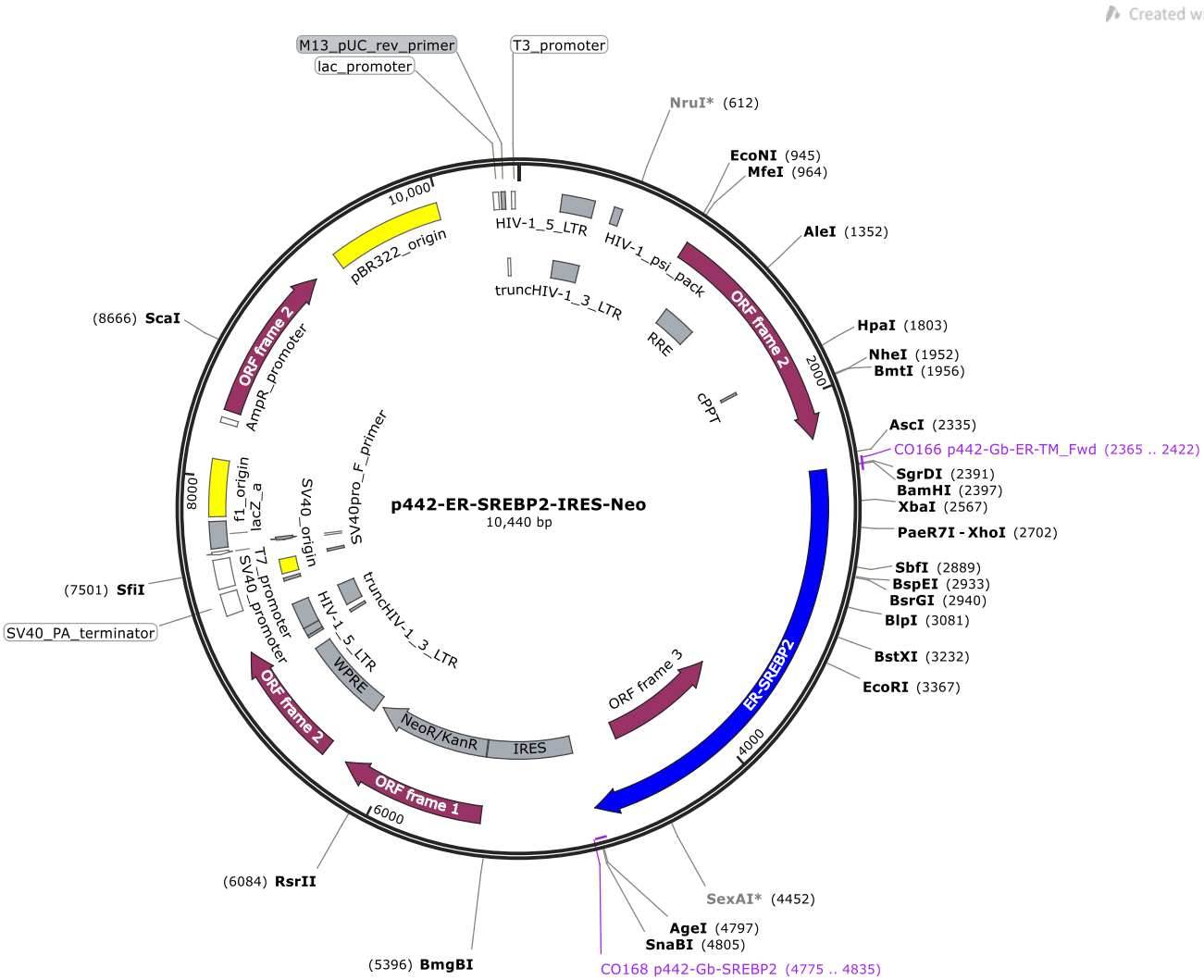

Figure 7. Vector map *Vector map of pKLV2U6gRNA5(BbsI)-PGKpuro2AZsG-W (addgene-67975) containing ER-SREBP2*

2.1.10 Cell lines

HT 1080: human fibrosarcoma cell line

A375: human melanoma cell line

UACC62: human melanoma cell line

LOX-IMVI: human melanoma cell line

M19: human melanoma cell line

Pfa1: 4-hydroxytamoxifen (TAM)-inducible Gpx4-/- murine immortalized fibroblasts

2.1.11 Computer software and online tools

Different application were used as bioinformatic tools: Excel 2016, GraphPad Prism 8.0, SparkControl™ Method Editor, SnapGene, https://genome.ucsc.edu/, https://www.uniprot.org/, http://crispor.tefor.net/, http://primer3.ut.ee/

2.2 Methods

2.2.1 Genomic methods

2.2.1.1 Gel purification of DNA fragments

DNA fragments were cut from agarose gels and purified using the Wizard® SV Gel and PCR Clean Up System (Promega) according to the manufacturer's protocol.

2.2.1.2 Restriction digest

Restriction enzymes (Bbs1 HF, Bst-BI, XhoI) were obtained from New England Biolabs GmbH and were used to prepare DNA plasmids for cloning. Reactions were set up in 50 µl according to manufacturer`s instructions.

2.2.1.3 Agarose gel electrophoresis

DNA fragments were separated according to their size by electrophoresis at 120 V in 1 or 2 % agarose gels in TEA 1x. Midori Green Advanced DNA Stain (NIPPON Genetics EUROPE) was added to the gel to enable visualization of the separated DNA fragments under a blue light or UV transilluminator. Gene Ruler 1 kb (Thermo Scientific) or Quantitas 200 bp-10 kb (Biozym) were used as a DNA ladder. Samples were mixed with 6x DNA loading dye (Thermo Fisher) if necessary and loaded in the gel pockets.

> **10x TAE buffer**: 0.4 M Tris-acetate (0.4 mM Tris-base and 5.71 % v/v acetic acid); 10 mM EDTA/NaOH pH 8.0

2.2.1.4 Isolation of bacterial plasmid DNA

After transformation of plasmid DNA, bacteria were allowed to form colonies (incubation for 16-20 h at 37 °C) on LB agar plates containing the corresponding antibiotic selection. Single colonies were picked from agar-LB plates with pipet tips. They were used to inoculate antibiotic containing LB medium (2 ml) and incubated overnight at 37 °C under constant shaking. Plasmid DNA was isolated from the bacterial culture on the next day using the QIAGEN plasmid Mini kit according to the manufacturer's protocol. Plasmid concentrations was measured on a NanoDrop 1000 Spectrophotometer.

2.2.1.5 Cell lysis for PCR analysis

For DNA extraction, the cells were trypsinized and then pelleted by spinning at 1500 rpm for 3 min. The supernatant was removed and the cells were washed with DPBS twice by centrifugation. After removing the supernatant, the pellet was resuspended in 150 µl of the lysis solution (Proteinase K [20 mg/ml] and TE-buffer (pH 8) at a ratio of 1:150). The sample was incubated at 55 °C for at least 1,5 h under constant shaking of 300 rpm. To stop the enzymatic reaction, the sample was heated to 95 °C for 2 min. The sample was stored at - 20 °C.

TE lysis buffer: 10 mM Tris-HCl (pH 8), 1 mM EDTA (pH 8), 50 mM KCl, 2 mM $MgCl_2$

2.2.1.6 Cloning of sgRNA guides

CRISPR spacer sequences were designed with the help of established online tools (http://crispor.tefor.net/). In order to clone the newly designed spacer sequences into the *Bbs*I digested backbone, pairs of DNA oligos were ordered (Invitrogen) containing the desired 20 bp spacers (N_{20}) with the addition of certain overhangs (see below in red).

Forward oligo: CACC(G)N_{20}
Reverse oligo: AAACN_{20}(complementary to forward oligo)(C)

Using *Bbs*I restriction sites it was possible to clone different spacer sequences (20-21 bp) that determine the CRISPR target. In a 50 µL reaction 2,5 µg pKLV2-U6gRNA5(BbsI)-PGKpuro2AZsG-W were digested with *Bbs*I at 37 °C for 1.5 h. The linearized vector band was isolated from a 1 % agarose gel, purified via gel extraction and the DNA concentration determined using the NanoDrop 1000 spectrometer. In parallel, the lyophilized oligos were dissolved in MilliQ H_2O to form stocks of 100 µM. 1 µL of the forward and reverse oligo stock was added to 100 µL TE-Buffer and the oligos were annealed by heating to 100 °C for 5 min before slowly cooling to RT. This procedure generated small fragments of double stranded oligos with matching overhangs to the digested (*Bbs*I) backbone which were used in ligation reactions (see 2.2.1.7). Chemical competent bacteria were transformed and single colonies were validated via Sanger sequencing (GATC Biotech).

2.2.1.7 Ligation of DNA fragments (T4-DNA-ligase)

The concentration of digested DNA fragments was measured using a NanoDrop 1000 Spectrophotometer. 50 ng of the backbone was mixed with the corresponding amount of insert DNA, T4-DNA-ligase and 10x ligase buffer according to the manufacturer's protocol. The ligation reaction was incubated for 20 h at 4 °C before being transformed into bacteria.

2.2.1.8 Genotyping of single clones

To determine if the single clones were knockouts for the target gene of the guides, the clones were screened by PCR. PCR amplification of the DNA target region was compared to the wild type cell's DNA. Any clones that have a shift inside of the amplicon were considered as KO. Therefor a PCR of lysed DNA was set up using the according genotyping forward and reverse primers.

Reaction mix

ddH_2O	18,625 µl
Forward primer [10 µM]	1,25 µl
Reverse primer [10µM]	1,25 µl
DreamTaq Green buffer [10x]	2,5 µl
dNTPs [40 mM]	0,25 µl
DNA [20 ng/µl]	1 µl
DreamTaq DNA Polymerase	0,125 µl

PCR protocol:

Step	Temperature	Duration	Cycles
Initial denaturation	95 °C	1-3 min	1
Denaturation	95 °C	30 sec	
Annealing	Tm-5 °C	30 sec	25-40
Extension	72 °C	1 min/kb	
Final extension	72 °C	5-15 min	1

PCR products were separated and visualized on a 1 % agarose gel.

2.2.1.9 Ligation of DNA fragments (Gibson cloning)

Gibson cloning is a DNA assembly method that enables the ligation of cut backbone vectors with blunt-end PCR products that have homologous arms. Therefore, primers were designed to amplify DNA fragments (inserts) that dispose at least 40 bp of overhang homologous to

the cut backbone vector. Q5 Polymerase was used in PCR reactions according to the manufacturer's protocol to achieve maximal sequence fidelity. The amplified inserts were purified using the Wizard® SV Gel and PCR Clean Up System (Promega). The vector DNA was linearized by restriction digestion and purified using the same clean up kit (Wizard® SV Gel and PCR Clean Up System (Promega)). The concentration and quality of all DNA fragments were assessed by the 1000 NanoDrop Spectrometer. The complete insert was cloned into pre double digested p442 neo (BstBI,XhoI). Therefor the linearized vector (~50 ng) and the inserts (~30 ng) were added to the HiFi DNA assembly mastermix (NEB) and incubated at 50 °C for 1 h according to the manufacturer's protocol. 2 µL of the reaction mix was used to transform chemical competent bacteria to allow amplification of the desired plasmid.

List of cloned vectors

Backbone	Insert
pBabe-puro ER™	SREBP1a N-term
pBabe-puro ER™	SREBP2 N-term

2.2.1.10 Amplification of DNA fragments for cloning

PCR reactions were set up in 25 µL containing the template DNA, gene-specific primers deoxynucleotides, Q5® High-Fidelity Buffer and DNA Polymerase.

Reaction mix:

ddH_2O	10,75 µl
Forward primer [10 µM]	1,25 µl
Reverse primer [10µM]	1,25 µl
Q5® High-Fidelity Buffer [5x]	10 µl
dNTPs [40 mM]	1 µl
DNA [20 ng/µl]	1 µl
Q5® High-Fidelity DNA Polymerase	0,25 µl

PCR protocol:

Step	Temperature	Duration	Cycles
Initial denaturation	98 °C	30 sec	1
Denaturation	98 °C	10 sec	
Annealing	52 °C	20 sec	30
Extension	72 °C	2 min 20 sec	
Final extension	72 °C	2 min	1

PCR products were separated and visualized on a 1 % agarose gel.

2.2.2 Methods working with bacteria

2.2.2.1 Preparation of chemical competent bacteria

The *E.coli* strain DH5α is provided by the research group of Ann Wehman. Bacteria Chemical competent cells were made by using the Z-Competent™ *E. coli* Transformation Kit & Buffer Set (Zymo Research) according to the manufacturer's protocol

2.2.2.2 Transformation of chemical competent bacteria

Several aliquots of chemical competent bacteria were thawed on ice and the plasmid DNA heated for 5 min at 60 °C. After thawing, 50 µL of the bacteria were each transferred to fresh 1.5 mL Eppendorf tubes and 2 µl of plasmid DNA was added. The samples were mixed gently and incubated on ice for 10 min before being exposed to a short (1 min) heat shock at 42 °C. Subsequently, 200 µL of S.O.C. medium was added to each tube and the bacteria were allowed to regenerate for 60 min at 37 °C before they were plated on LB agar plates containing ampicillin (100 µg/ml). LB plates were incubated overnight at 37 °C until single colonies appeared.

2.2.2.3 Liquid Cultures

Single colonies were picked from agar-LB plates with pipet tips. Subsequently the tip was tossed in a 10 ml tube with 2 ml LB-media and 2µl of ampicillin (100 µg/ml). The tube was incubated over night at 37 °C. After incubation, the liquid culture was used for mini prep and the back-up plate was sealed with para film and stored at 4 °C.

2.2.3 Methods of gene transfer

2.2.3.1 Lipofection

For the transfection of cells with plasmid DNA, $1x10^5$ cells were plated on a 6 cm-plate. The next day, the cells were transfected using a liposomal based system (X-tremeGENE HP-DNA Transfection Reagent (Roche)). Each transfection mix contains a combination of two different plasmids (0,5 µg each) targeting an up and downstream site from the certain region. Subsequently, 2 µl of the transfection reagent was added and the mix was vortexed for 15 sec and incubated at 25 °C for 15 min. The transfection mix was added dropwise to the cell cultures. After 24 h a correlated antibiotic was added to start the selection of the transfected cells.

2.2.3.2 CRISPR/Cas9-mediated KO

For generating knockouts stable Cas9 transduced cell lines were used. The genomic sequence of the targeted genes to be knocked out were retrieved using the UCSC Genome Browser. A region with essential exons for the enzyme activity was chosen. Using CRISPor platform, guide RNAs were designed and selected considering their predicted activity and off-target score. Initially, two guides were chosen for a cut upstream of the targeted sequence and two guides for a cut downstream of it. Subsequently, correlated genotyping primers were designed using the NCBI primer design tool whereas paying attention that the primers have a distance of approximately 100 bp to the PAM sequence to avoid damaging their binding site. For each strategy, a forward and a reverse oligonucleotide was assayed.

2.2.3.3 Generating KO clones of DHCR7 and SC5D

Single sgRNA guides (**Table 1**) were designed to target critical exons of the genes to be inactivated. Guides were cloned into the BbsI-digested pKLV U6gRNA(BbsI)-PGKpuro2aBFP vector (Addgene #50946).

Table 1 List of generated knockouts

Parental cell line	Cell line name	Target gene	sgRNA
HT1080 _Cas9	HT1080 DHCR7_KO	hDHCR7	GAA GAAGTAGCCC TTGACCAG, TTG CAGGTGCCCT CCAGGCGG
HT1080 DHCR7_KO	HT1080 DHCR7/SC5D_KO	hSC5D	CAT GTGGCTGGAT ACACGTAG, GAT GTCATCTTCT GGCCATGG
UACC62_Cas9	UACC62 DHCR7_KO	hDHCR7	GAA GAAGTAGCCC TTGACCAG, TTG CAGGTGCCCT CCAGGCGG

HT1080 and UACC62 cells were infected with VSV-G pseudotyped lentiviral particles containing the transfer plasmid lentiCas9-Blast and selected with blasticidin. $2x10^5$ cells stably expressing Cas9 protein were seeded on a 6-well plate and cultured for 24 h. On the next day, cells were co-transfected with the desired sgRNA expressing plasmids (pKLV-U6gRNA1 PGKpuro2aBFP) using the X-tremeGENE HP agent according to the manufacturer's recommendations (Roche Diagnostics). After incubation of the cells for 24 h the DNA intake was checked under the fluorescence microscope. The transfected cells are visible as the transfection vector expresses a blue fluorescent protein. In case of a successful transfection, the medium was changed to standard DMEM containing 2 µg/ml of puromycin. As a control, one plate of untransfected cells was treated in the same way. The selection medium was changed every 24 h until the transfected cells were confluent. Subsequently, 60 cells were plated on a 96-well-plate for single-cell cloning and incubated at low oxygen. The medium was refreshed every four days. At confluence, clones were expanded and genotyped via PCR (see 2.2.1.8).

2.2.3.4 Generating re-expression clones of DHCR7/SC5D

To re-express DHCR7 and SC5D, HT1080 DHCR7/SC5D KO cells were transduced with a lentivirus expressing the corresponding proteins. Therefor the cDNA with a FLAG tag was cloned from pcDNA3.1+/C-(K)DYKvector (GenScript ORFs) into p442 backbone.

Original backbone	Insert
pcDNA3.1	hDHCR7-Flag
pcDNA3.1	hSC5D-Flag

The FLAG tag is a short hydrophilic protein tag that is easily recognized by the anti-FLAG antibody, which enables the detection of proteins via Western Blot. Because of its small size, the FLAG tag does not interact with other proteins.

2.2.3.5 Preparation of lentiviral particles for overexpression of genes

HEK 293T cells were used to produce replication-incompetent lentiviral particles pseudotyped with the ecotropic envelope protein of the murine leukaemia virus (MLV) or the pantropic envelope protein VSV-G. A third generation lentiviral packaging system consisting of a transfer plasmid (lentiCas9-Blast (Addgene #52962), p442-Mock, p442-Puro-hDHCR7, p442-Neo-hSC5D, pBabe-puro ER™- SREBP2 N-term), pRSV-Rev, pHCMV-MLV and pHCMV-VSV-G was co-lipofacted into HEK 293T cells. Viral particles containing cell culture supernatants were harvested 48 h after transfection and used to transduce the cell line of interest.

2.2.4 Cell culture

2.2.4.1 Standard cell culture methods

The cells were cultured in Dulbeco's Modified Eagle Medium (DMEM) [1x] + GlutaMAX (gibco) supplemented with 10 % fetal bovine serum (FBS) (Corning) and 1 % Pen-Strep (Lonza). Cell culture incubators were operated under humid conditions at 37 °C with 5 % of CO_2. For culturing 10 cm and 6 cm plates (Sarstedt) as well as 6 to 96-well plates (Sarstedt) were used according to the number of cells required. Unless otherwise stated the cells were split at a rate of 1:5 three times a week and media were changed every two days or if necessary. Therefor the growth medium was removed, cells were washed with DPBS to remove residual culture medium and trypsinized using Trypsin-EDTA (0.05 %) for 5 min. Trypsinization was stopped by adding standard DMEM and a fraction of the detached cells was transferred to a fresh cell culture vessel already containing standard DMEM medium. Passage numbers were recorded.

Standard DMEM: DMEM, 10 % FBS, 1 % glutamine, 50 U/ml penicillin G, 50 µg/mL streptomycin

2.2.4.2 Preparation of delipidated medium

To remove serum lipids and lipids-derived metabolites from our standard DMEM, FBS was aliquoted and treated with silica (5 g silica/50 ml FBS). The flasks were put in the incubator shaker for 3 h at 4 °C and subsequently centrifuged at 2000 x g at 4 °C for 20 min. The supernatant was transferred to new flasks and after a second treatment with silica (5 g silica/50 ml FBS) incubated for 16 h at 4 °C. Thereafter the FBS was centrifuged at 2000 x g at 4 °C for 20 min and filtered.

2.2.4.3 Freezing and thawing of cells

If required, cells were thawed in a water bath at 37 °C. To remove residual DMSO, cells were washed in 5 ml of standard DMEM and centrifuged to discard the supernatant. Cell pellets were resuspended in 10 mL standard DMEM and seeded onto a 10 cm cell culture plate. Cryo-conserved cell stocks could be prepared when cells reached roughly 80 % confluency. Therefor cells were trypsinized, pelleted at 1500 rpm for 5 min and resuspended in DMEM containing 10 % DMSO. 1 mL aliquots were filled into cryo vials and stored at -80 °C overnight in Mr. Frosty™ to a slow freezing process (-1 °C/min). The cryo vials were transferred to a liquid nitrogen tank for long term storage the next day.

2.2.4.4 Determination of cell numbers

Cells were harvested by standard trypsinization and diluted in DMEM. Cell suspension, 10 µl, was used to determine cell number using the Neubauer improved chamber.

2.2.4.5 Drug treatment of cells

To analyze cell viabilities of the used cell lines under different conditions, cells were treated with ferroptosis inducer RSL3. Therefor 3000 or 4000 cells per well were plated on a 96-well plate at a volume of 100 µl per well. The plate was put in the incubator for 6 h to let the cells attached. Afterwards, the medium was refreshed and compounds (Cholesterol, 7-DHC, Lathosterol, RB38, Tasin, Tamoxifen) added if necessary. The cells were incubated for 18, 24 or 48 h, as indicated in the results, depending on the added compound and then treated with RSL3 at following concentrations: 0, 10, 25, 50, 100, 200, 400 and 800 nM (final concentration in the well).

2.2.4.6 Cell viability assays

AquaBluer method

Cell viability was performed in 96-well plates 24 h or 48 h after RSL3 treatment using AquaBluer (Resazurin sodium salt) as an indicator of viable cells according to the manufacturer's recommendations (Sigma-Aldrich). Therefor culture medium was replaced by DMEM containing 0,5 % AquaBluer and cells were incubated for 2 h. Then 540ex/590em was measured by a Spark multimode microplate reader (TECAN).

2.2.5 Protein analysis

2.2.5.1 Protein extraction

To collect proteins from cultured cells, the cells were trypsinized and then pelleted by spinning at 1500 rpm for 3 min. The supernatants were removed and the cells were washed with DPBS twice after centrifuging a second time. Subsequently, the pellet was supplemented with 80 µl of Protease Inhibitor combined with Ripa Buffer and stored at -20 °C overnight. The next day, the samples were thawed on ice for 30 min and then centrifuged at 10000 x g at 4 °C for 30 min.

> **Ripa Buffer** (pH 8): 20 mM Tris hydrochloride, 150mM NaCl, 1mM EDTA, 1% NP-40, 1mM EGTA, 1% sodium deoxy cholic acid sodium salt

2.2.5.2 Protein quantification

The protein concentration was valuated with the Pierce BCA Protein Assay Kit (Thermo Scientific) according to the manufacturer's protocol. Eight samples of standard protein concentrations from 0 to 1 mg/ml were used and after 30 min incubating at 30 °C, the samples were measured at 562 nm with a Spark multimode microplate reader (TECAN).

2.2.5.3 Sodium dodecyl sulfate polyacrylamide gel electrophoresis

20 µg of protein was supplemented with 4 µl loading dye [4x] and filled up with Ripa buffer to a volume of 16 µl. The samples were stored at -20 °C. Prior to electrophoresis, samples were thawed on ice for 5 min and then denatured for 5 min at 70 °C. As standard, we used 10 µl of PageRuler Plus Prestained Protein ladder (Thermo Scientific). Proteins were separated in a PerfectBlue^{TM} Vertical Double Gel System electrophoresis chamber filled with running buffer. The samples run at 70 V in the stacking gel, as soon as the samples reached the separation gel, voltage was increased to 100 V.

SDS-buffer[10x] (pH8,3): Tris base 30 g, glycine 144g, SDS 10g, H_2O 1l.
loading-buffer[6x]: 9 % SDS, 50% Glycerol, 0,03 % Bromophenol Blue, 9% ß-Me, 375 mM Tris pH 6,8.

	separation gel [12%]	**stacking gel [5%]**
D. water	3,35 ml	1,68 ml
Tris buffer (1,5M, pH 8,8)	2,5 ml	1,25 ml
Acrylamide [40%]	4 ml	2 ml
SDS [10%]	100 µl	50 µl
APS [10%]	50 µl	25 µl
TEMED	15 µl	15 µl

SDS gels were liberated from their plastic scaffold and proteins were transferred to a PVDF (polyvinylidene difluoride) membrane for subsequent Western blot analysis or directly used for Coomassie staining.

2.2.5.4 Coomassie staining of SDS gels

SDS gels were liberated from their plastic scaffold rinsed with TBST and put in a sealable container suitable for microwave heating. The gel was covered with Coomassie staining solution, sealed and heated in the microwave for 2 min at maximum power until the staining solution boiled. Subsequently, the container was put on a rocking table for 5-10 min for cooling. The Coomassie staining solution was removed and the gel was washed with H_2O several times until the desired level of de-staining was attained (incubation overnight). Stained protein bands were documented using the c400 Visible Fluorescent Western System (Azure biosystems).

Coomassie staining solution: 0.1% Brilliant Blue R250, 12,5% acetic acid, 45% methanol, 10% acetic acid, 42,5% H_20

2.2.5.5 Western blot analysis

After protein samples have been separated by SDS-PAGE, proteins were transferred to a PVDF membrane using the mixed molecular weight protocol (60 min, 12 V) on the semi-dry PerfectBlue™ Electro Blotter Transfer System (Peqlab). Membranes were cut depending on the size of the protein of interest to allow simultaneous detection of a marker protein. Subsequently, membranes were blocked with 5 % skim milk in TBST for at least 60 min. Primary antibodies were added in 5 % skim milk according to the manufacturer's protocol

and applied overnight at 4 °C under constant motion. On the next day, membranes were washed two times in TBST for 10 min and incubated with HRP-conjugated secondary antibodies at room temperature for 2 h in TBST containing 5 % skim milk. Membranes were washed four times in TBST and proteins were visualized by application of WesternBright ECL HRP Substrate (Advansta) following the manufacturer's instruction. The c400 Visible Fluorescent Western System (Azure biosystems) was used for imaging and documentation. If necessary, antibodies were stripped from the PVDF membrane with 0.2 M NaOH for 8 min to allow the application of a different primary antibody. After stripping, membranes had to be blocked again with 5 % skim milk for 60 min before the whole hybridization and developing procedure could be repeated.

TBST: 25 mM TRIS, 125 mM NaCl, 0.1 % Tween-20, pH 7.6
Transfer buffer: SDS-buffer containing 10 % methanol

2.2.6 Determination of cholesterol metabolites using liquid chromatography–mass spectrometry (LC-MS)

All the LC/MS analysis were performed by Werner Schmitz (Biocenter Hubland, University of Würzburg).

2.2.6.1 Preparation of cellular extracts

To prepare cellular extracts, cells were washed, trypsinized and $1x10^6$ cells centrifuged to remove the supernatant. The pellet was washed twice with DPBS and stored at –20 °C. 190 µl MeOH and 47 µl H_2O were added to resuspend the pellet. The sample was mixed properly by using an ultrasonic cup horn. Subsequently, 20 µl of a standard solution containing 7-DHC-d7 (1 mM) and cholesterol-d7 (1 mM) in MeOH/$CHCl_3$ (1/1, v/v) was added. Afterwards, 30 µl HCl (0.2 M), 90 µl $CHCl_3$, 100 µl $CHCl_3$ and 100 µl H_2O were added in order. The sample was mixed after each step and centrifuged (15000 rpm, 2 min) lastly. The lower phase was transferred to a new Eppendorf Cup and dried at 45 °C under a stream of nitrogen gas.

2.2.6.2 Separation of cholesterol and cholesterol esters

The dry residue was resuspended in 150 µl hexane, centrifuged and the hexane phase was transferred to a Strata SI-1 Silica Column (55 µm, 70 A, 100 mg/1 ml, Phenomenex). Initially, unbound compounds (FOa) were eluted by adding 750 µl hexane. Next, 750 µl

hexane/acetic acid ethylester (18/1, v/v) was added to elute cholesterol esters (FCE). Subsequently, 750 µl hexane/acetic acid ethylester (9/1, v/v) was added to elute contaminants (FOb). The column was blown out and finally, 750 µl hexane/acetic acid ethylester (9/1, v/v) was added to elute cholesterol to get the free cholesterol-containing fraction (FFC). The column was blown out and the FFC was evaporated at 45 °C under a stream of nitrogen.

2.2.6.3 LC/MS-analysis of cholesterol

The dry eluate samples were redissolved in 50 µl isopropyl alcohol and centrifuged for 2 min at 15000 rpm. For LC/MS-analysis, 20 µl of the supernatants were transferred to sampler-vials and 3 µl were applied to an C8 column assembly at 40 °C (Acclaim C8 pre-column, 5 µm particles, 10 × 2 mm; Acclaim RSLC C8 column, 2.2 µm particles, 50 × 2.1 mm, Thermo Scientific) and isocratically eluted for 30 min. Acetonitrile/H_2O/formic acid (90/9.9/0.1, v/v/v) was used as mobile phase with a flow rate of 350 µl/min. The eluent was directed to the ESI source of a Q Exactive mass spectrometer (QE-MS) from 7 min to 13 min after sample injection. LC/MS analysis was performed on a Thermo Scientific Dionex Ultimate 3000 UHPLC system hyphenated with a QE-MS equipped with a HESI probe (Thermo Scientific). The data was acquired using tSIM in positive mode with: range - m/z 369.35 and m/z 367.34; resolution - 70,000; microscans - 1; AGC-Target – 1e6; maximum injection time – 400 ms; and the follow HESI Source Parameters: heath gas (30); auxiliary gas (10); sweep gas (3); spray voltage (2.5 kV); Capillary temperature (320 °C); S-lens RF level (55.0) and Aux Gas Heater temperature (120°C). Peaks corresponding to the calculated ion masses (± 2 mMU) were integrated using TraceFinder software (Thermo Scientific).

2.2.7 Data presentation and statistical analyses

Data are presented as mean ± s.d. unless stated otherwise. As a general rule for the cell-based experiments, the graphs show the mean ± s.d. of n = x wells (x values are given in the figure legends) representative of a single experiment performed independently y times (y value is given in figure legends) for reproducibility. Statistical analysis was performed using GraphPad Prism 8.0 software.

3 Results

3.1 CRISPR-based genomewide screen identified novel ferroptosis regulator

To investigate ferroptosis regulating processes, specific aspects that are associated with ferroptosis sensitivity or resistance need to be identified. CRISPR-based genetic screens provide techniques for functional analysis of whole genomes. Pooled sgRNA libraries enable the generation of cellular pools containing single mutants for a given gene, which can then be phenotypically interrogated. Thus, it is possible to analyze gene functions and their corresponding cellular processes. Our group while still at the Helmholtz Zentrum München applied a CRISPR-based genetic screen on ferroptosis sensitive cells and besides the known gene ACSL4, the screen revealed DHCR7 as a novel ferroptosis regulating gene (**Figure 8**). Thus, uncovering a new regulatory node that I have provided initial insight into its function as depicted in the forthcoming sections.

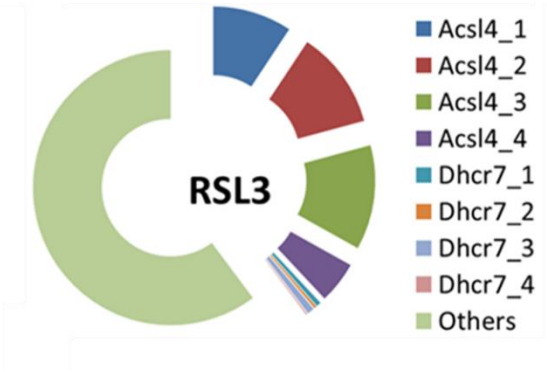

Figure 8. Identification of DHCR7 as a new pro-ferroptotic gene *Relative counts of gRNAs identified in the cell pool selected with ferroptosis inducer RSL3. ACSL4 was already identified using 1st generation libraries[1].*

3.2 DHCR7 and SC5D deficiency

Cholesterol constitutes a main structural component of plasma membranes and is required for variety of functions in different organisms, which includes the synthesis of steroid hormones, neurosteroids, bile acids and Hedgehog family proteins that are essential for developmental signaling [69, 70]. The biosynthesis of cholesterol entails a complex series of biochemical reactions encompassing more than 30 intermediates and regulating enzymes. **Figure 10A** depicts a scheme of the final steps of cholesterol biosynthesis. 7-dehydrocholesterol reductase (DHCR7) catalyzes the last step of this biosynthetic pathway, converting 7-dehydrocholesterol (7-DHC) to cholesterol. 7-DHC differs from cholesterol only by the presence of a unsaturation between C7-8 [71] (**Figure 9**). The importance of this last step is highlighted by a series of monogenic disorders in enzymes involved in the

production of cholesterol[72]. Potentially the best characterized is the Smith-Lemli-Opitz syndrome (SLOS) which is a disorder characterized by DHCR7 mutations. Given the proposed connections between cholesterol biosynthesis and ferroptosis regulating mechanisms the now recognition that DHCR7 is a potential hub point, the question arises to what extent DHCR7 and the previous enzyme sterol-c5-desaturase (SC5D) affect ferroptosis.

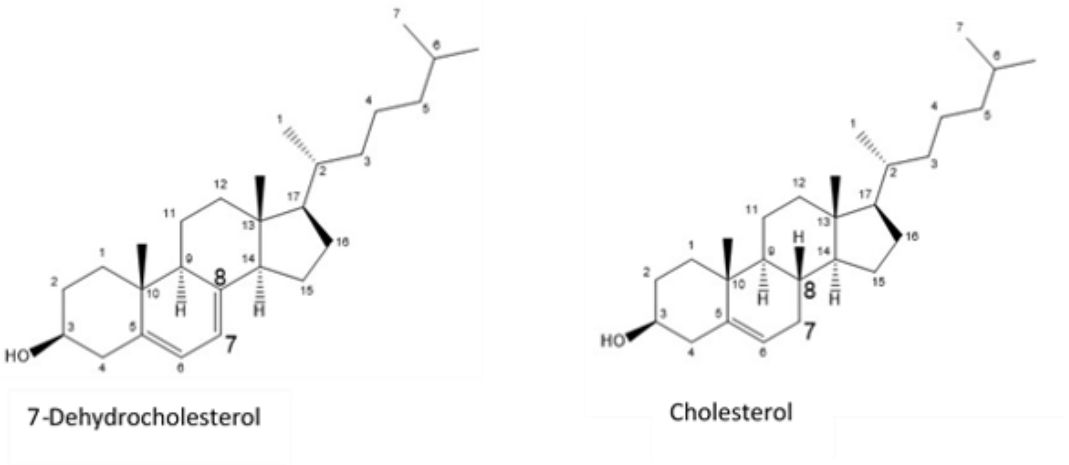

Figure 9. Structural formula of 7-Dehydrocholesterol and Cholesterol

To assess the impact of DHCR7 and SC5D and their substrates, the group while still in Munich used CRISPR/Cas9 to generate in the ferroptosis sensitive cell HT1080 cells specifically lacking DHCR7 and a combination of DHCR7 and SC5D, the latter occurred during work on this thesis. It is assumed that cells lacking DHCR7 do not convert 7-DHC to cholesterol and cells showing deficiency of both DHCR7 and SC5D are unable to metabolize lathosterol nor 7-DHC. We initially assessed the sensitivity of this newly generated cell towards the ferroptosis inducer RSL3 [39]. (**Figure 10B**) While the HT1080 DHCR7/SC5D double KO cells are similarly sensitive to the parental HT1080 Cas9 cells, cells presenting only deficiency in DHCR7 have a pronounced resistance towards RSL3. To assess the absence of the sterols of interest, we quantified their levels in the respective cell lines - HT1080 Cas9, DHCR7_KO and DHCR7/SC5D_KO. (**Figure 10C**) As predicted, cholesterol was detectable in all cell lines, whereas 7-DHC is just detectable in the DHCR7_KO cell line and DHCR7/SC5D_KO cells are the only ones presenting detectable levels of lathosterol. Worth pointing out that the remaining cholesterol detected in all cell lines is likely arising from the serum in which the cells are grown. In order to unequivocally prove that the cell do

synthesize cholesterol experiments using isotopically labeled glucose would be required and will be performed prior to submission of the manuscript.

These results strongly suggest that DHCR7 and SC5D deficiency has an impact on cell viability and affects the intracellular sterol composition. Also suggesting that increased amount of 7-DHC provides a strong cytoprotective effect on the HT1080 cell line.

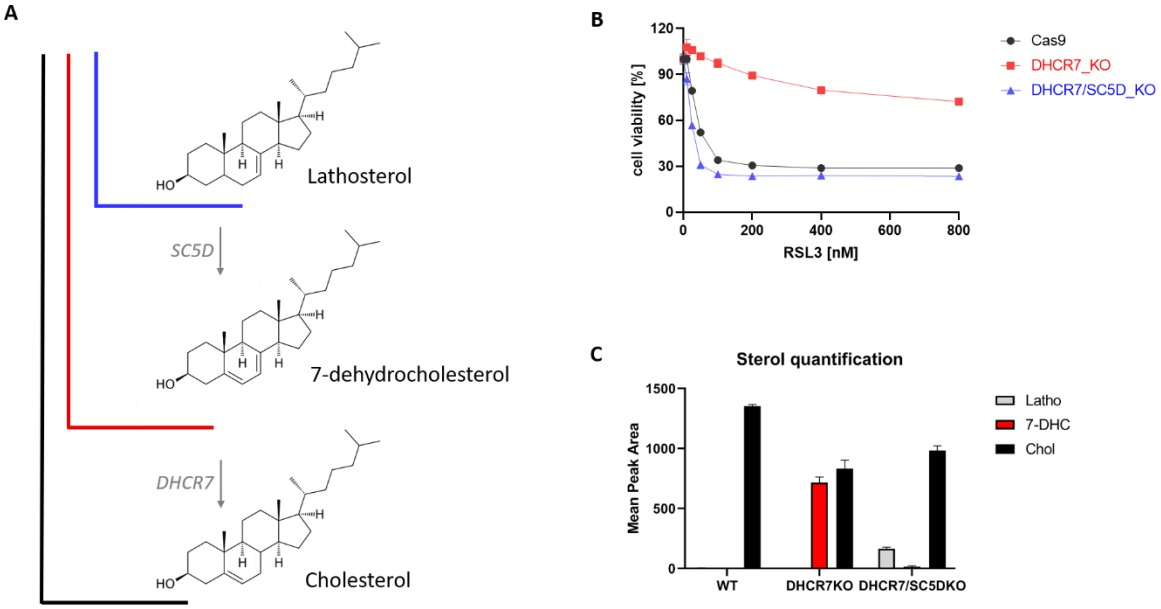

Figure 10. DHCR7 and SC5D deficiency A *Partial scheme of cholesterol biosynthesis. SC5D catalyzes the conversion of lathosterol to 7-DHC, DHCR7 converts 7-DHC to cholesterol.* ***B*** *Enzyme knockout affects cell viability. HT1080 Cas9, DHCR7_KO and DHCR7/SC5D_KO cells were treated with ferroptosis inducer RSL3. Cell viability was assessed by using AquaBluer 48 h after treatment. Data shown represent the mean ± s.d. of n = 4 of a 96-well plate from a representative experiment performed independently three times.* ***C*** *Sterol quantification of HT1080 Cas9, DHCR7_KO and DHCR7/SC5D_KO cells. Data shown represent the mean ± s.d. of n = 3 samples from a representative experiment performed once.*

3.2.1 Sterol effect

Lathosterol is an intermediate of cholesterol biosynthesis and its serum level correlates with cholesterol synthesis in cells containing the intact biosynthetic pathway [73]. 7-DHC, the direct precursor of cholesterol, is highly oxidizable and gives rise to a series of oxysterols that have been proposed to contribute to SLOS [74]. Our results support that an increased amount of 7-DHC due to deficiency of DHCR7 has rather a protective effect against ferroptosis inducers. Now it remains to be demonstrated whether the addition of exogenous sterols can phenocopy the genetic deletions. To assess the impact of exogenous sterols under the different genotypes we used the previously described HT1080 DHCR7_KO and DHCR7/SC5D_KO cell lines

and supplemented them with lathosterol and 7-DHC before the treatment with RSL3 (**Figure 11**). Overall, the treatment with lathosterol or 7-DHC presented a similar effect. The HT1080 Cas9 cells presented a higher viability when treated with either lathosterol or 7-DHC. Regarding the DHCR7_KO cell line, this effect was even more pronounced. As the HT1080 DHCR7/SC5D_KO cells cannot metabolize neither lathosterol nor 7-DHC, no protective effect was evidenced. Surprisingly, even 7-DHC supplementation was unable to *protect* the double KO line. In order to gain more insights if any of the used sterols modulate known regulators of ferroptosis we assessed protein expression levels of key regulators of ferroptosis. **Figure 11B** shows representative immunoblots of the different cell lines exposed to the different sterols. Overall, we did not notice any marked changes in the known antiferroptotic regulators (GPX4 and AIFM2). Nevertheless, it is worth mentioning that the ACSL4 level in HT1080 DHCR7_KO cells without treatment and treated with cholesterol is decreased. ACSL4 is an essential enzyme for ferroptosis and the decreased expression could partially account for the increased resistance.

In conclusion we demonstrate that 7-DHC accumulation as well as exogenous supplementation of 7-DHC presented an antiferroptotic activity in the HT1080 cell line.

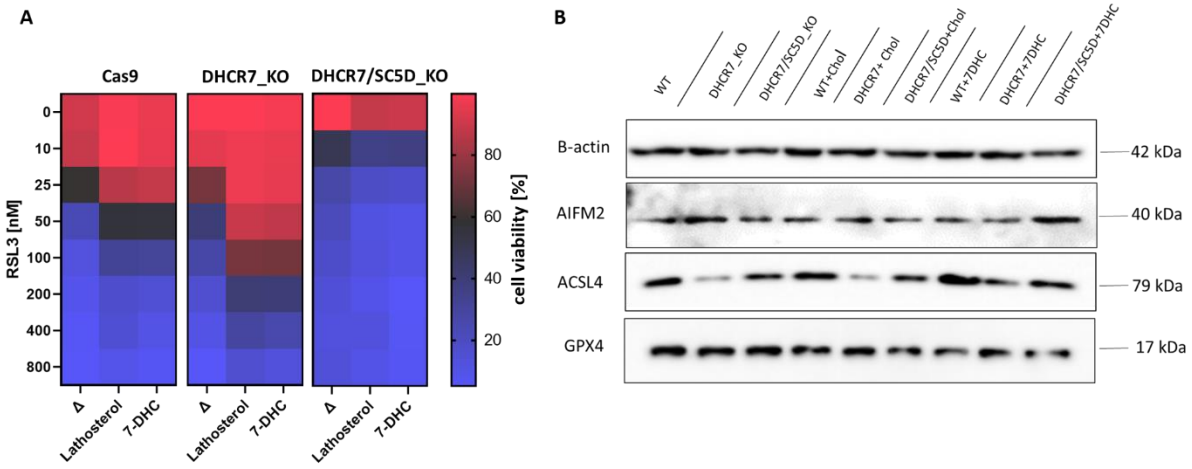

Figure 11. Sterol effect on DHCR7 and SC5D deficiency A *Heat map showing cell viabilities of HT1080 Cas9, DHCR7_KO and DHCR7/SC5D_KO cells. Cells were incubated with sterols (10 µM) for 16 h and then treated with ferroptosis inducer RSL3. Cell viability was assessed by using AquaBluer 48 h after treatment. Data shown represent the mean ± s.d. of n = 4 of a 96-well plate from a representative experiment performed independently three times.* ***Δ****: without any sterol* ***B*** *Western blots showing protein levels of HT1080 Cas9, DHCR7_KO and DHCR7/SC5D_KO cells treated with sterols (10 µM). Uncropped images of blots are shown in Supplementary figure 1.*

3.3 Selenium impact

Selenium is an essential trace element required for several critical cellular functions. Its biological relevance is accounted for the biosynthesis of the 21st amino acid selenocysteine (Sec), which is incorporated in selenoproteins that function in their vast majority as oxidoreductases and are involved in defense mechanisms in different organisms [75]. Among 25 identified human selenoproteins, there is the family of glutathione peroxidases [76]. Glutathione peroxidase 4 (GPX4) is a key enzyme for antioxidant defense and reduces lipid hydroperoxides to their corresponding alcohols [77]. As during the course of this thesis, we noticed that upon changing the fetal bovine serum (FBS - used to supplement cell culture media) batches some of the effects we initially observed were less prominent (**Figure 11A** – unsupplemented conditions). For instance, the protective effect due to the loss of DHCR7 was markedly decreased. This effect ultimately turned out to be associated to variations of selenium content in different FBS batches. In order to approach this, we investigated the consequences of supplementing Se to our FBS "Se-Low". Initially, we set to address if selenium affects cell viability and whether selenium has any impact on the 7-DHC level.

For this purpose, we cultured HT1080 WT and DHCR7_KO cells in medium supplemented with sodium selenite (Na_2SeO_3 - NaSe, 25 nM) and treated them with the GPX4 inhibitor RSL3. The cell viabilities were compared to those performed in standard medium. (**Figure 12A**) Both the WT and the DHCR7_KO cells cultured with NaSe were markedly more resistant to RSL3. We next reassessed the effect of lathosterol and 7-DHC in selenite supplemented conditions. (**Figure 12B**) Compared to the previous experiment performed in standard medium (**Figure 11A**), the protective effect of lathosterol and 7-DHC in the WT and DHCR7_KO cells was markedly increased, maintaining the previous trend. But remarkably, in the presence of sodium selenite the exogenous supplementation of 7-DHC was markedly protective in the double KO cell line. Suggesting that 7-DHC is rapidly consumed in selenium poor conditions – a feature that will be discussed in the following sections. **Figure 12C** shows the relative sterol quantification of HT1080 Cas9 and DHCR7_KO cells. The 7-DHC/Cholesterol ratio in DHCR7_KO cells is significantly higher than in the wildtype cell line. As the previous results show that there might be a correlation between selenium and 7-DHC levels, we next performed western blots of HT1080 Cas9, DHCR7_KO and DHCR7/SC5D_KO cells and compared samples without and plus addition of 7-DHC. Cells were cultured in standard medium and medium supplemented with NaSe. As expected, the expression of the selenoproteins GPX1 and GPX4 are markedly increased in presence of selenium. These results re-emphasize the protective effect of 7-DHC and confirm that selenium is required for GPX4 expression and its function to reduce peroxidized lipids. Peroxidized lipids can generate detrimental radicals that potentially consume endogenous antioxidants, such as 7-DHC. At low selenium levels, GPX4 function is restricted and 7-DHC is constantly consumed. Consequently, when cells are challenged with a ferroptosis stimuli, there is no effective level of 7-DHC to suppress lipid peroxidation and associated cell death.

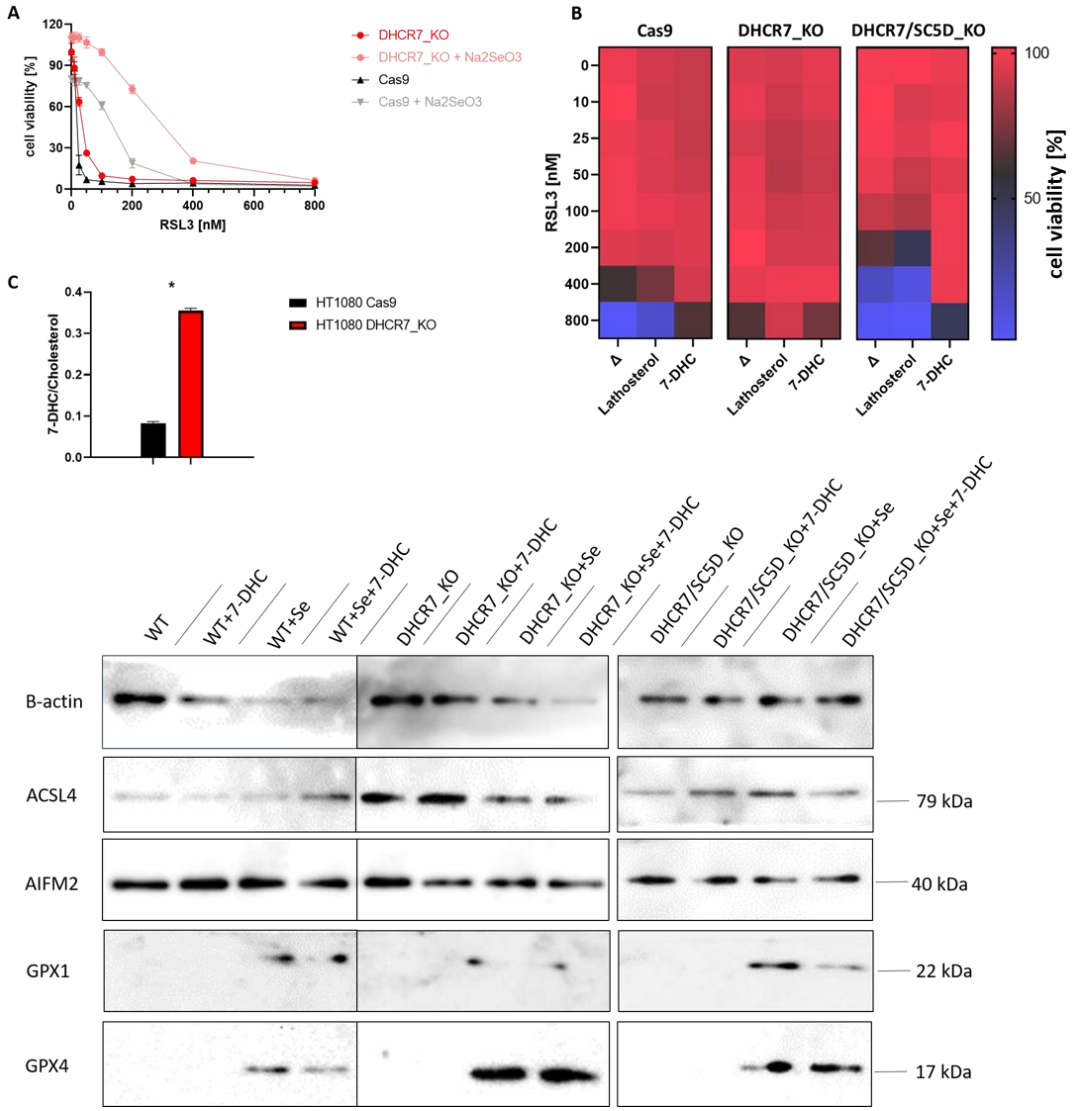

Figure 12. Selenium impact A *Medium supplemented with NaSe (25 nM) affects cell viability of HT1080 Cas9 and DHCR7_KO cells. Cells were treated with ferroptosis inducer RSL3. Cell viability was assessed by using AquaBluer 48 h after treatment. Data shown represent the mean ± s.d. of n = 3 of a 96-well plate from a representative experiment performed independently three times.* ***B*** *Heat map showing cell viabilities of HT1080 Cas9, DHCR7_KO and DHCR7/SC5D_KO cells cultured in medium supplemented with NaSe (25 nM). Cells were incubated with sterols (10 µM) for 16 h and then treated with ferroptosis inducer RSL3. Cell viability was assessed by using AquaBluer 48 h after treatment. Data shown represent the mean ± s.d. of n = 4 of a 96-well plate from a representative experiment performed independently two times.* ***Δ****: without any sterol* ***C*** *7-DHC/Cholesterol ratio of a relative sterol quantification of HT1080 Cas9 and DHCR7_KO cells. Cells were cultured in medium supplemented with NaSe (25 nM) and 10^6 cells were counted for the measurement. Data shown represent the mean ± s.d. of n = 3 samples from a representative experiment performed once.* *******P<0.0001 (paired t test)* ***D*** *Western blots showing protein expression of HT1080 Cas9, DHCR7_KO and DHCR7/SC5D_KO cells. Cells were cultured in standard medium and medium supplemented with NaSe (25 nM). Uncropped images of blots are shown in Supplementary figure 2.*

3.4 Re-expression of DHCR7 and SC5D

Since it is known that variations due to cell clonality could arise during the single cell cloning step of the CRISPR generated lines, we used the double KO lines and reconstituted them sequentially with a lentiviral vector expressing SC5D or DHCR7 as depicted in **Figure 13**[78].

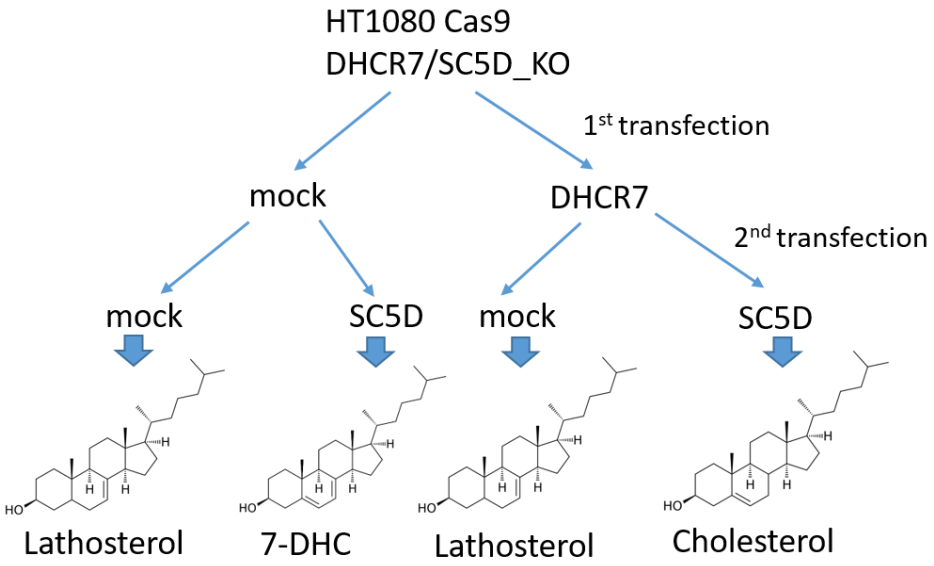

Figure 13. Cell generation *Scheme of re-expression of DHCR7 and SC5D in HT1080 DHCR7/SC5D_KO cells and their main metabolites*

Re-expression of SC5D rendered cells markedly resistant to RSL3 and this was accompanied by an increase in the endogenous levels of 7-DHC (**Figure 14**). In order to further support the importance of 7-DHC in blocking ferroptosis we took a pharmacological approach using Tasin-1. Tasin-1 inhibits the Emopamil-Binding Protein (EBP), an enzyme involved in cholesterol biosynthesis that catalyzes the conversion of Δ^8-sterols (e.g. zymostenol) to their corresponding Δ^7-isomers (e.g. lathosterol). Supportive of the role of 7-DHC in suppressing ferroptosis only cells able to produce and accumulate 7-DHC were sensitized to treatment with Tasin-1. Along the same lines, re-expressing both DHCR7 together with SC5D decreased the levels of 7-DHC, as well the protective effect conferred by SC5D re-expression alone. Detailed characterization of the sterol composition is depicted in **Figure 14C**. Since we anticipated that due to its intrinsic reactivity, 7-DHC could be reacting with lipid radicals during the course of ferroptosis and thus supporting membrane integrity, we assessed the levels of 7-DHC upon RSL3 treatment. After 6 h of treatment with 200 nM RSL3 we noticed

a small but significant decrease in the total level of 7-DHC (**Figure 14B**). Indicative of it has been consumed upon triggering ferroptosis and also underscoring the notion that not all the 7-DHC pool is consumed but it is potentially an intracellularly confined fraction.

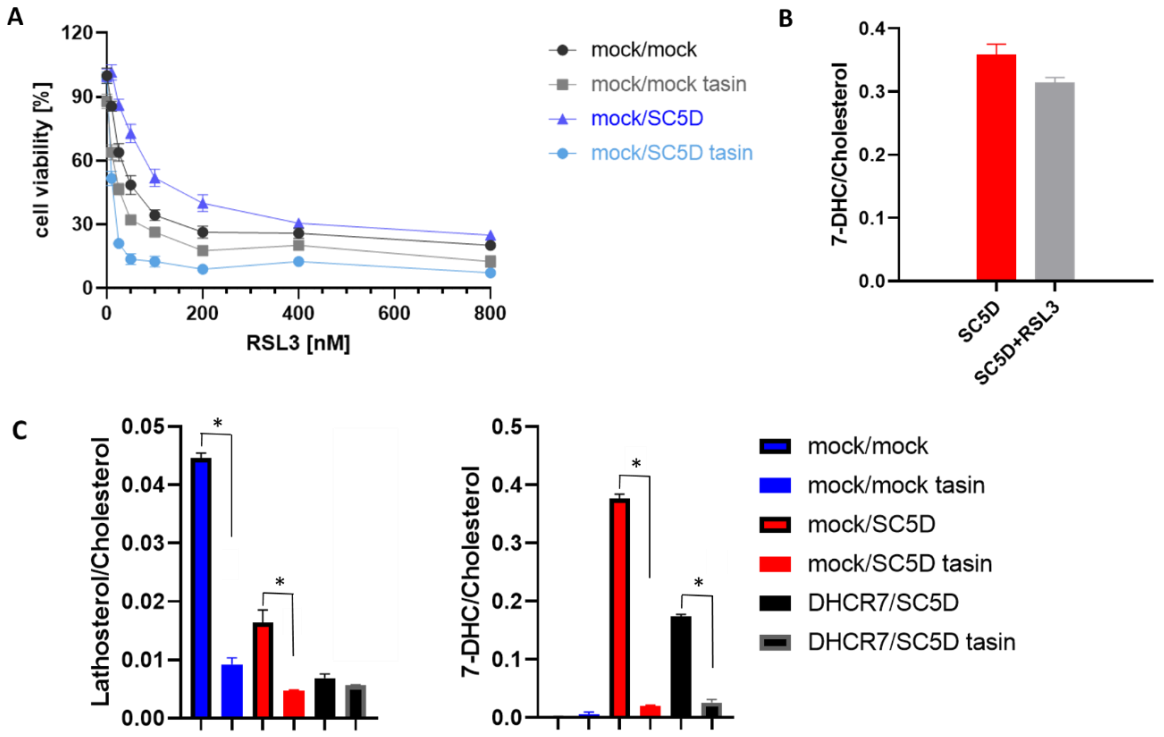

Figure 14. Re-expression of DHCR7 and SC5D in HT1080 DHCR7/SC5D_KO cells A *Treatment with tasin affects cell viabilities of HT1080 DHCR7/SC5D_KO cells and HT1080 DHCR7/SC5D_KO cells re-expressing SC5D. Cells were cultured in medium supplemented with NaSe (20 nM) and treated with ferroptosis inducer RSL3. Cell viability was assessed by using AquaBluer 48 h after treatment. Data shown represent the mean ± s.d. of n = 6 of a 96-well plate from a representative experiment performed once.* ***B*** *7-DHC/Cholesterol ratio of a relative sterol quantification. 10 ^{6} cells were plated and treated with 200 nM of RSL3 for 6 h. Cells were cultured in medium supplemented with NaSe (10 nM). Data shown represent the mean ± s.d. of n = 2 samples from a representative experiment performed independently two times.* ***C*** *Lathosterol- and 7-DHC/Cholesterol ratio of relative sterol quantifications. Cells were cultured in medium supplemented with NaSe (20 nM) and treated with 500 nM of tasin for 48 h. 10^{6} cells were counted for the measurement. Data shown represent the mean ± s.d. of n = 3 samples from a representative experiment performed once.* ***P<0.0001 (one-way ANOVA)***

Next, we also addressed the effect of Se supplementation in the cells described above. To inspect the effect of selenium, we performed western blots and compared protein levels of cells cultured in standard medium and in medium supplemented with NaSe (**Figure 15A**). As expected, the expression of the selenoproteins GPX1 and GPX4 was markedly increased in the presence of selenium. The ACSL4 expression in HT1080 double knockout cells re-expressing SC5D and re-expressing both enzymes cultured with NaSe presented a marginal decrease, which could partially account with the increased resistance of these cell lines. The relative sterol quantification (**Figure 15B**) of cells cultured in medium supplemented with NaSe demonstrates that the addition of selenium was sufficient to increase the steady-state levels of the metabolites analyzed. The significant increase of 7-DHC in cells re-expressing SC5D cultured with NaSe is especially remarkable and enhances the assumption that selenium affects cell viability and that there is a synergistic effect of 7-DHC. The increase of lathosterol and cholesterol after addition of NaSe suggests that selenoproteins could support sterol synthesis.

In summary, evidence is provided that indeed 7-DHC protects from ferroptosis and that it is consumed readily in condition where GPX4 is insufficient. Moreover, our results are suggestive that 7-DHC protects a specific subcellular location from intracellular lipid peroxidation. Suggestive that ferroptosis is executed in a defined subcellular location rather than an overwhelming state of lipid peroxidation.

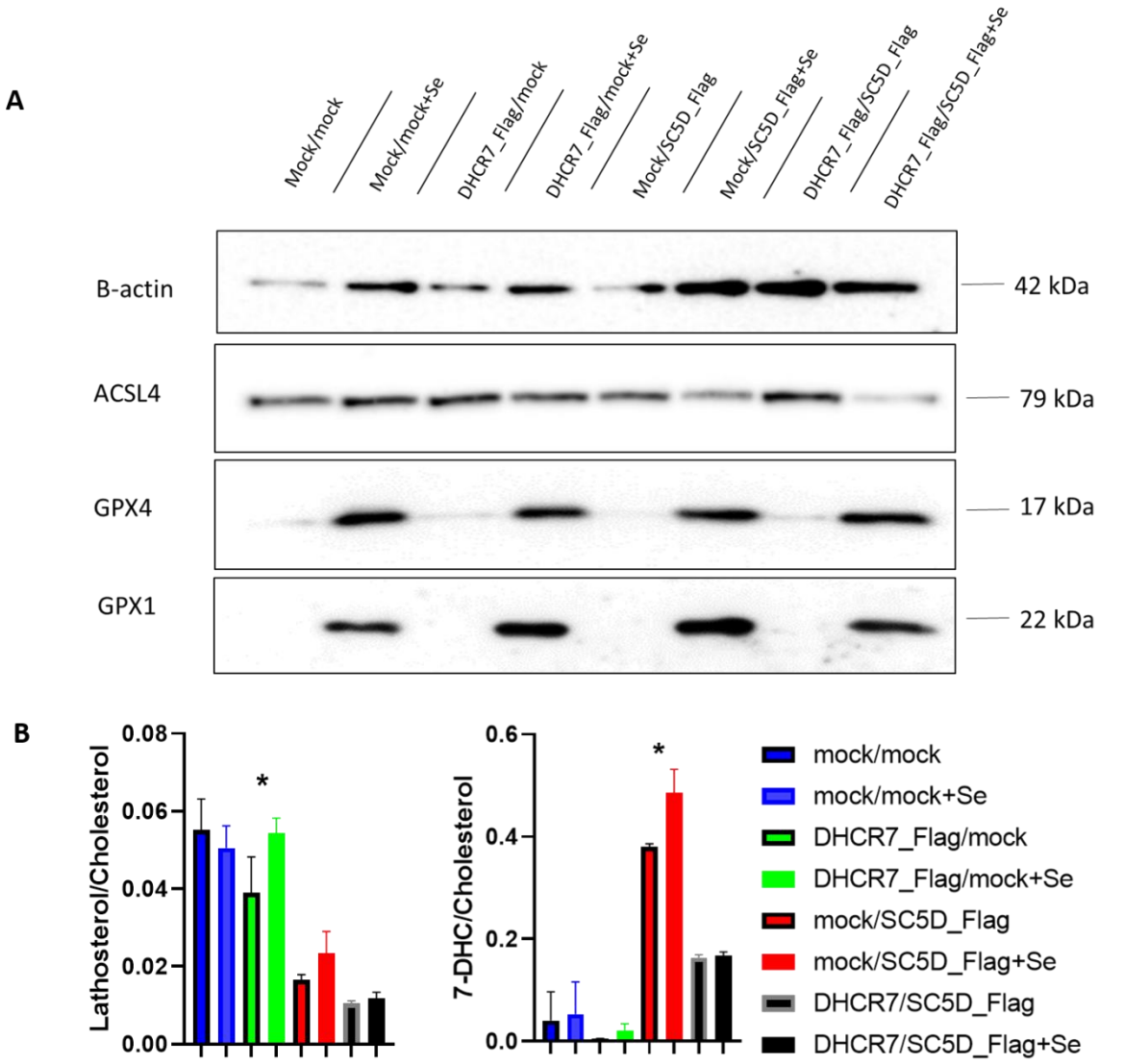

Figure 15. Selenium affects re-expression of DHCR7 and SC5D A *Western blot showing protein levels of HT1080 DHCR7/SC5D_KO cells with re-expression of DHCR7 and SC5D. Cells were cultured in standard medium and medium supplemented with NaSe (25 nM). Uncropped images of blots are shown in Supplementary figure 3* ***B*** *Lathosterol- and 7-DHC/Cholesterol ratio of relative sterol quantifications. Cells were cultured in standard medium and medium supplemented with NaSe (25 nM). 10^6 cells were counted for the measurement. Data shown represent the mean ± s.d. of n = 3 samples from a representative experiment performed once.* ***P<0.0001 (one-way ANOVA)***

3.4.1 Pharmacological inhibition of DHCR7

In order to validate the pharmacological tractability of DHCR7 to modulate ferroptosis sensitivity we used a series of described DHCR7 inhibitors. AY9944 and BM 15.766 are known and commonly used DHCR7 inhibitors. As AY9944 also inhibits additional enzymes of the cholesterol biosynthesis and the inhibition effect of BM 15.766 is not entirely sufficient, several investigations were made in the meantime to provide a specific and effective inhibitor of DHCR7 [79], [80], [81]. The research group of Prof. Dr. Peter Imming (Institute for pharmacy, Halle) provided us a compound named RB38 that inhibits DHCR7. To validate the inhibition effect, we treated HT1080 Cas9 cells with RB38 and assessed their response to RSL3 **(Figure 16A)**. Treatment with RB38 leads to an increased resistance against ferroptosis induced by RSL3. Similar to previous results, NaSe supplemented medium enhances the protective effect. **Figure 16B** further shows that RB38 presents a dose response effect, thus appearing to be an effective inhibitor of DHCR7 in cells.

As such, we can conclude that RB38 could be a suitable tool to explore to what extent DHCR7 could be inhibited to block ferroptosis. At this stage, one could envisage its use in the context of ischemia reperfusion where ferroptosis was proposed to play a role [82].

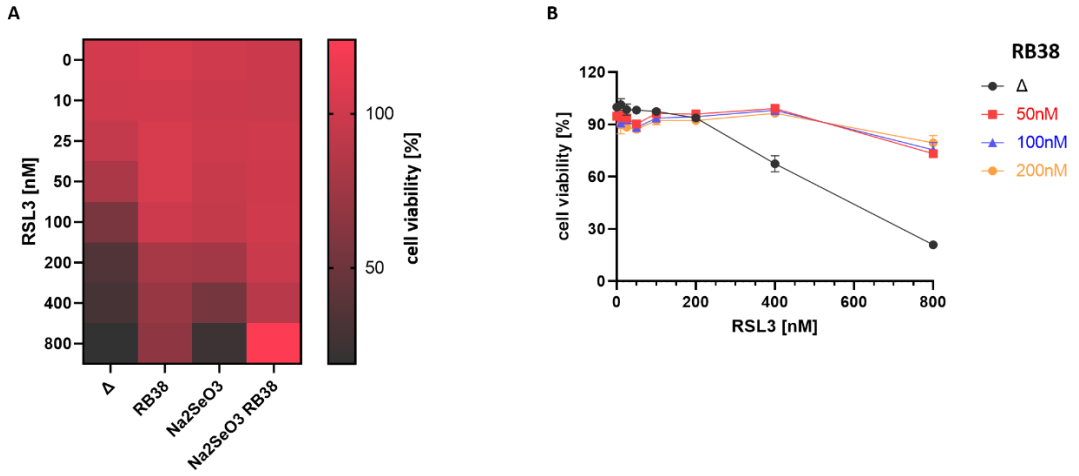

Figure 16. Pharmacological inhibition of DHCR7 A *Heat map showing cell viability of HT1080 Cas9 cells. Cells were incubated with DHCR7 inhibitor RB38 (200 nM) for 24 h and then treated with ferroptosis inducer RSL3. The experiment was performed in standard medium and medium supplemented with NaSe (10 nM).* ***Δ****: standard medium without RB38* ***B*** *RB38 is a dose response DHCR7 inhibitor. Cell viabilities were assessed by using AquaBluer 48 h after treatment. Data shown in* ***A*** *and* ***B*** *represent the mean ± s.d. of n = 3 samples from a representative experiment performed once.*

3.4.2 Compound sensitivity

In the last few years, there has been substantial progress in the field of ferroptosis regulation. By now, there are known numerous pathways and compounds that modulate ferroptosis. As the previous experiments were all performed with just GPX4 inhibitor RSL3, the question arises how cells showing DHCR7 or SC5D deficiency behave when treated with other cytotoxic compounds.

In order to approach this, a panel of cytotoxic drugs was assessed in the different cell lines. For this we used FIN56, a pro-ferroptotic compound that activates squalene synthase (FDFT1) and induces GPX4 degradation [54]. ML210 inhibits GPX4 and Erastin inhibits the system x_c^-, a cystine-glutamate antiporter that is necessary for the biosynthesis of the antioxidant tripeptide glutathione (GSH) [39], [83]. Besides ferroptosis inducing compounds, we treated the cells with Bortezomib and Carfilzomib, cytostatic anticancer drugs acting as proteasome inhibitors [84], [85]. Furthermore, we used Auranofin which is an antirheumatic drug inhibiting several leucocyte activating pathways, for example the selenoprotein thioredoxin reductase [86]. **Figure 17** shows cell viabilities of HT1080 DHCR7/SC5D_KO cells re-expressing DHCR7 and SC5D treated with these different compounds. Regarding treatment with RSL3, FIN56, ML210 and Auranofin, HT1080 double knockout cells that re-express SC5D are the most resistant towards ferroptotic stimuli, whereas non-ferroptotic stimuli showed limited correlation with the genotypes.

Ultimately, these results demonstrate that there is a tendency of HT1080 DHCR7/SC5D_KO cells re-expressing SC5D, thus accumulating 7-DHC, to be more resistant against ferroptosis inducing compounds. This protective effect is not translated to a general resistance as the other compounds present no marked effect.

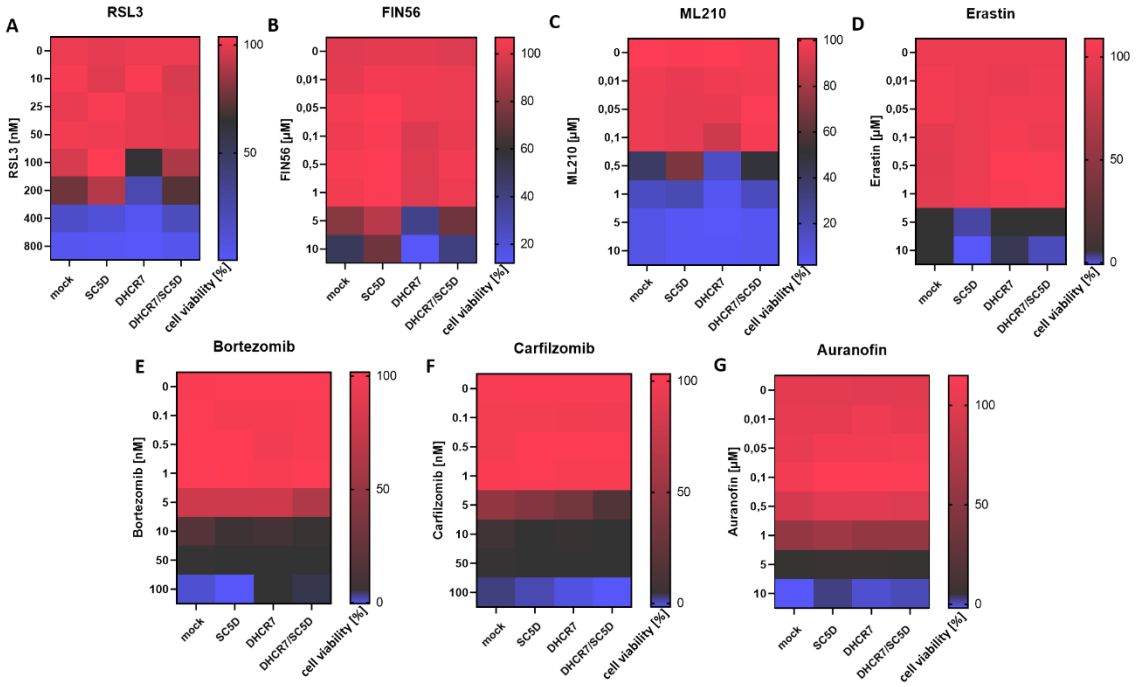

Figure 17. Compound sensitivity *Heat maps showing cell viabilities of HT1080 DHCR7/SC5D_KO cells re-expressing DHCR7 and SC5D. Cells were cultured in medium supplemented with NaSe (25 nM) and treated with ferroptosis inducing (**A-D**) and cytotoxic (**E-G**) compounds. Cell viability was assessed by using AquaBluer 72 h after treatment. Data shown represent the mean ± s.d. of n = 6 of a 96-well plate from a representative experiment performed once.*

3.5 Impact on different cell lines

In order to provide an initial appraisal of the broad relevance of our finding we aimed to test the impact of the antiferroptotic activity of 7-DHC in different cell lines. For this purpose, we used three melanoma cell lines. To validate the impact of 7-DHC on these melanoma cell lines, we incubated the cells with 7-DHC and subsequently treated them with ferroptosis inducer RSL3. This experiment was performed in both standard medium and medium supplemented with NaSe. (**Figure 18**) In all cell lines tested, addition of 7-DHC presented a dose response protective effect. Supplementation with NaSe results in a further increased resistance of the UACC62 and A375 cells, whereby it has to be mentioned that RSL3 barely kills A375 cells. Of notice, under selenium poor condition adding 7-DHC to the LOX IMVI cell line provided a strong protective effect, suggestive of the inherent sensitivity of this cell to ferroptosis. Similar to the effect of 7-DHC, NaSe increased the viability of LOX IMVI cells.

In conclusion, we can state that despite the overall different sensitivities, 7-DHC can act as potent pro-survival sterol in all cell lines tested, recapitulating the results obtained with the model cell line HT1080.

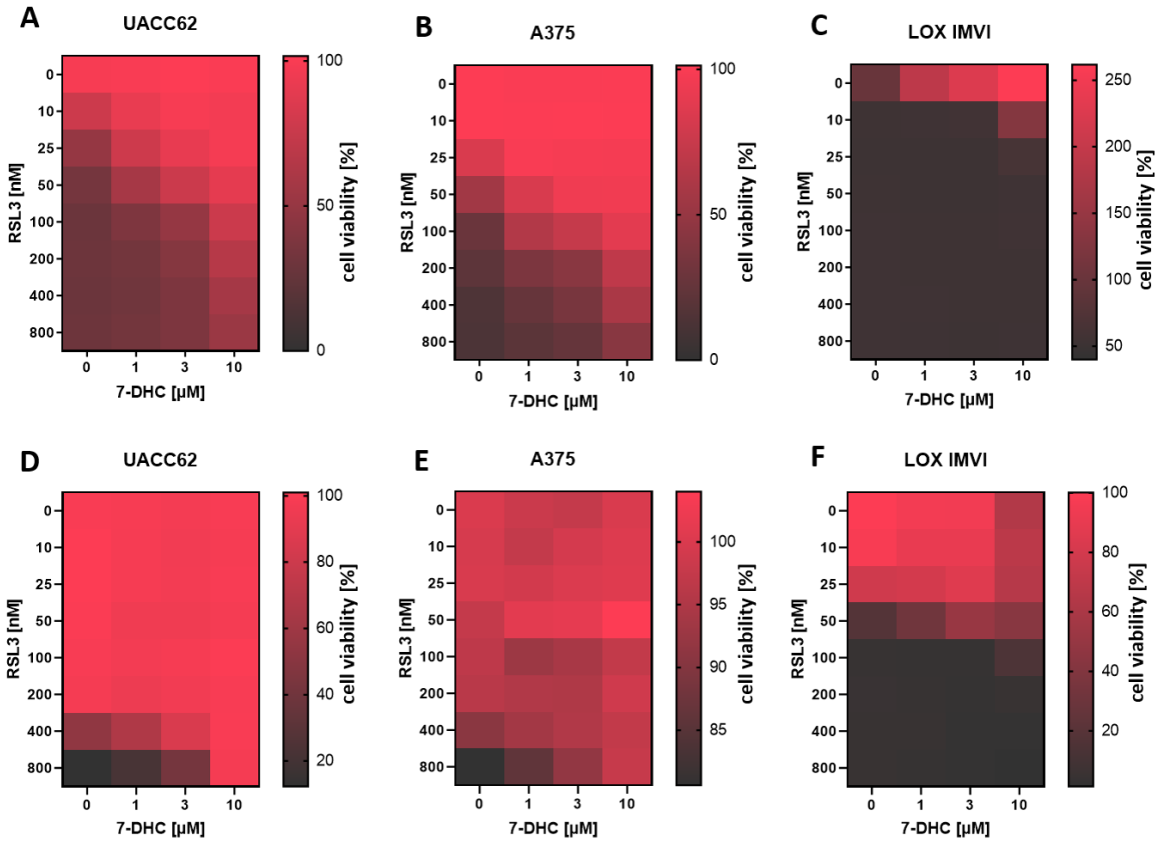

Figure 18. Impact on different cell lines *Heat maps showing cell viabilities of different melanoma cell lines incubated with 7-DHC for 16 h and then treated with ferroptosis inducer RSL3. Experiments were performed in standard medium (**A**-**C**) and medium supplemented with NaSe (25 nM) (**D**-**F**). Cell viability was assessed by using AquaBluer 48 h after treatment. Data shown represent the mean ± s.d. of n = 3 of a 96-well plate from a representative experiment performed once.*

3.6 Genetic model of GPX4 deficiency

The Cre/loxP system is a genetic tool for gene targeting based on the site-specific recombinase Cre (cyclization recombination) which catalyzes the recombination between two artificially inserted loxP (locus of crossing over of bacteriophage P1) sites. The gene of interest is floxed (flanked with lox) to be recognized by Cre . To improve the Cre/loxP system and to provide temporal control on the genetic deletion, inducible CreER recombinases have been developed. The CreER recombinase contains a mutated hormone-binding domain of the estrogen receptor that can be activated by tamoxifen (TAM) [88]. The CreER/loxP system is well applicable for modulation of genes involved in ferroptosis. Given that so far, we only approached ferroptosis induced pharmacologically, it stands to be demonstrated that 7-DHC has a protective effect also in a genetic model.

As such we used an inducible GPX4 knockout mouse line previously generated [89], [41]. This mouse embryonic fibroblast cell line (namely, Pfa1) contains two loxP flanking the 3´UTR of GPX4. These cells further express CreERT2 allowing the conditional deletion of GPX4 upon TAM supplementation in the growing media. Therefore, to induce GPX4 deletion, the cells were incubated with TAM and then treated with cholesterol, lathosterol and 7-DHC. We performed the experiments in standard medium and medium supplemented with NaSe to validate the effect of selenium on cell viability. (**Figure 19A**) TAM decreases cell viability significantly compared to the cells without TAM in all conditions. As it can be noticed, cholesterol does not show any notable effect. Unlike cholesterol, lathosterol and 7-DHC both were able to protect the cells. This effect is detectable in standard medium and NaSe supplemented conditions. At present, the protective effect of lathosterol is not entirely understood but it is not without reasoning that it could be effectively converted to 7-DHC, but this would require that it is not further metabolized. Therefor further studies are needed. Moreover, lathosterol and 7-DHC protect GPX4 deficient cells in a dose dependent manner. **Figure 19B** depicts a western blot demonstrating the deletion of GPX4 and that the sterols did not impact on this process.

To sum up, it is to mention that the TAM induced GPX4 deficiency based on CreER/loxP is a good tool to study ferroptosis regulating compounds as it is not directly influenced by drug dependent metabolism. Ultimately, our results corroborate our previous data showing that 7-DHC could also protect cells in a genetic model of ferroptosis. Further supporting its function as an important antiferroptotic metabolite.

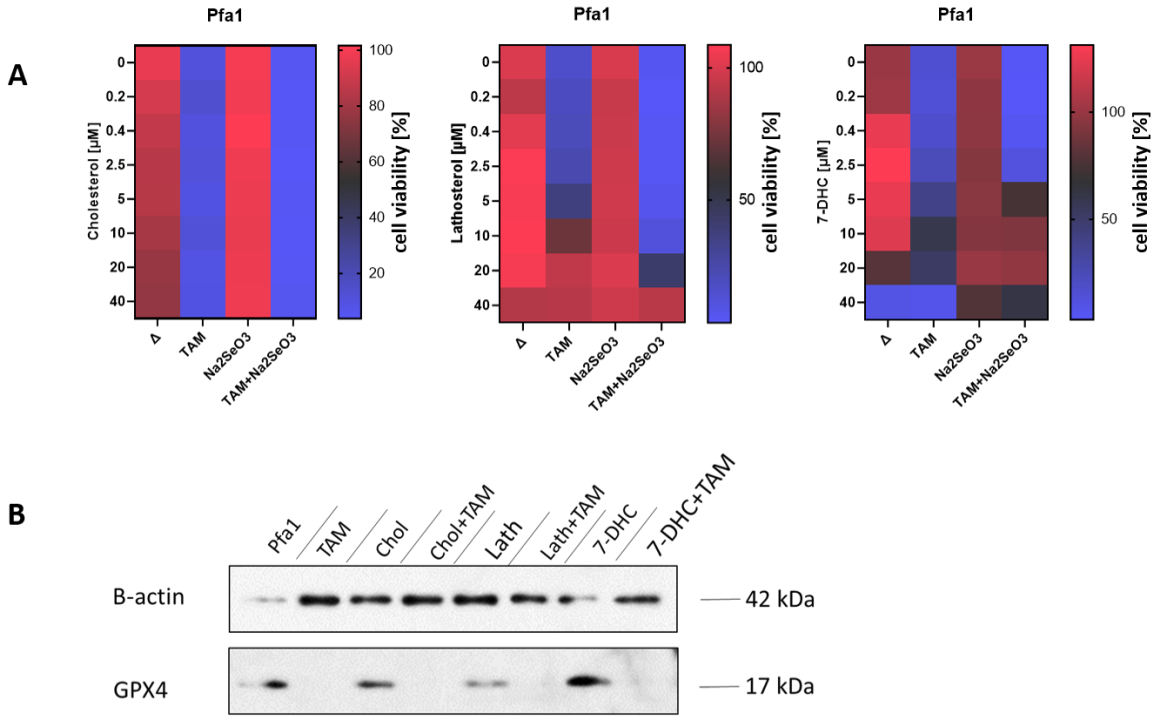

Figure 19. Genetic model of GPX4 deficiency A *Heat maps showing cell viabilities of Pfa1 cells treated with cholesterol, lathosterol and 7-DHC. Gpx4 was disrupted by the addition of 1 µM of Tamoxifen (TAM) and the experiments were performed in standard medium and medium supplemented with NaSe (25 nM). Cell viability was assessed by using AquaBluer 48 h after treatment. Data shown represent the mean ± s.d. of n = 3 of a 96-well plate from a representative experiment performed once.* ***Δ****: standard medium without TAM* ***B*** *Western blot showing protein levels of Pfa1 cells treated with sterols. GPX4 was efficiently depleted on TAM treatment. Uncropped images of blots are shown in Supplementary figure 4*

3.7 Impact of delipidated medium

All biochemical reactions are based on demand and supply of substrates and products. In cell culture the major source of cholesterol is the FBS used to supplement growth media. As the available cholesterol affects lipid metabolism and cholesterol biosynthesis via activation of SREBP transcription factor family members, the question arises to what extent there is a correlation between serum composition and activity of DHCR7. We envisaged that using serum low in sterols would force our cells to rely on their biosynthetic machinery and ultimately impact on the parameters we have been assessing. Therefore, in the next set of experiments we explored the impact of delipidated serum on viability and sterol levels on the cell lines we generated.

To evaluate the lack of sterols in the delipidated medium and its effects, we first prepared a batch of serum lacking sterol by treating the standard FBS with activated silica overnight to remove lipids. The estimated sterol content of the FBS after treatment (delipidated) is shown in **Figure 20A**. **Figure 20B** shows cell viabilities of cells in delipidated media. Surprisingly, we observed that HT1080 DHCR7/SC5D_KO cells are extremely sensitive to this condition and readily die. Interestingly, this effect could be rescued by cholesterol, liproxstatin-1 (Lip-1) and re-expression of SC5D. Suggestive that 7-DHC is an important prosurvial molecule for cancer cells undergoing this kind of metabolic stress. To picture to what extent delipidated medium affects sterol levels, we next performed a relative sterol quantification of the two cell lines (**Figure 20C**), taking into account the sterol content of the FBS. Regarding the amount of cholesterol, there was no significant difference. The amount of lathosterol and 7-DHC in samples prepared in delipidated medium is clearly increased compared to standard medium supportive of an increased biosynthetic rate.

To summarize, these results demonstrate the significance of sterol supply by the FBS. Whereby low sterols stimulate biosynthesis and push the cell towards an anabolic state and thus enhancing the effect of the enzyme knockouts. Moreover, we uncover an unexpected sensitivity of cells lacking SC5D to delipidated conditions, moreover the rescue by Lip-1 suggests that this form of cell death is related to ferroptosis. Thus, further studies will be required in order to characterize this novel mechanism of ferroptosis induction.

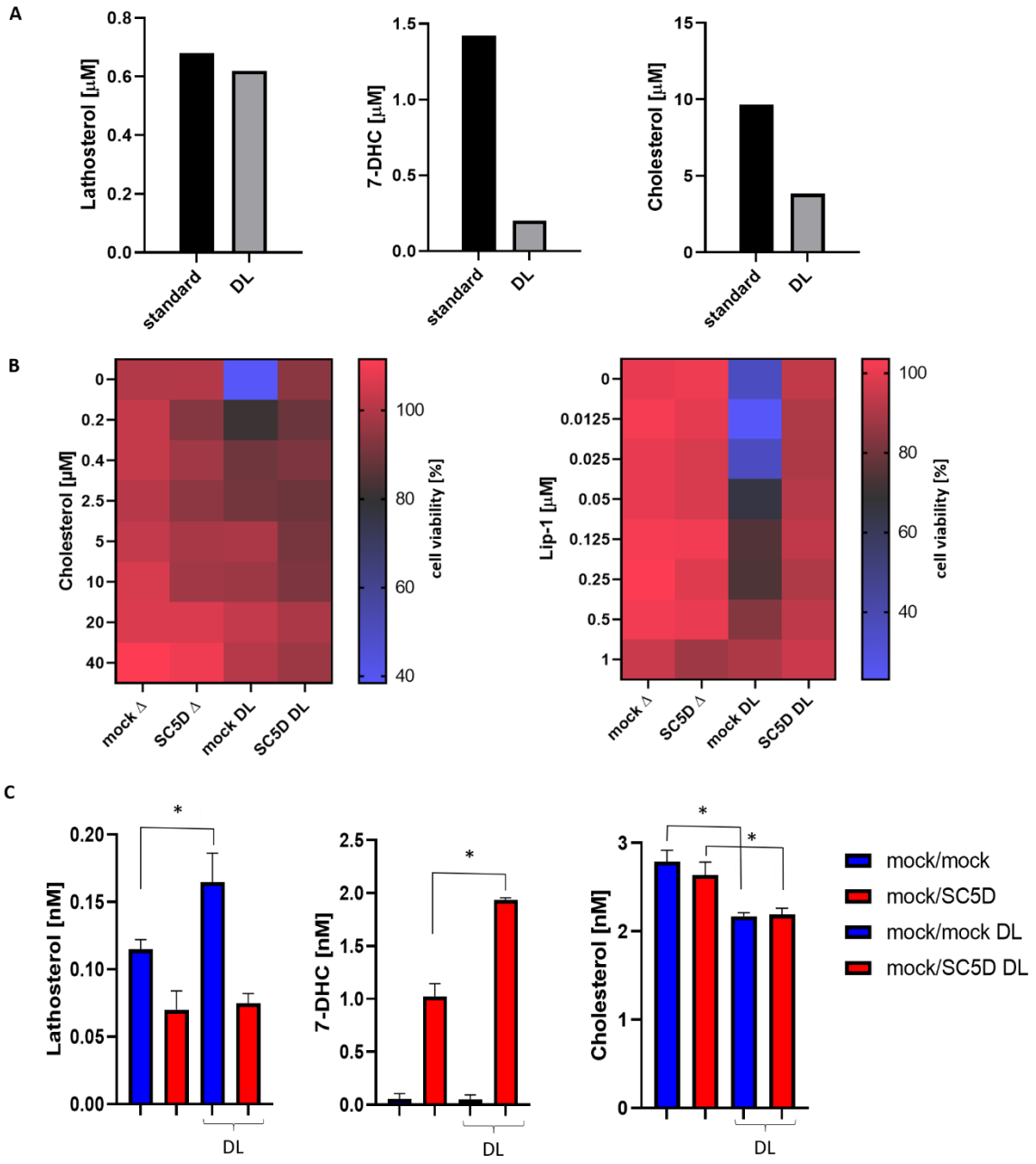

Figure 20. ***Impact of delipidated medium A*** *Sterol composition of standard medium and delipidated medium* ***B*** *Cell viabilities of HT1080 DHCR7/SC5D_KO mock/mock and mock/SC5D treated with Lip-1 and cholesterol. Cells were cultured in standard medium and delipidated medium. Cell viability was assessed by using AquaBluer 48 h after treatment. Data shown represent the mean ± s.d. of n = 3 of a 96-well plate from a representative experiment performed independently two times.* ***C*** *Relative sterol quantification of HT1080 DHCR7/SC5D_KO cells cultured in standard medium and delipidated medium. 10^6 cells were counted for the measurement. Data shown represent the mean ± s.d. of n = 2 samples from a representative experiment performed once. *P<0.0001 (one-way ANOVA)*

4 Discussion

The importance of cell death including its essential function for human health and diseases is undeniable. Thus, understanding and exploiting cell death mechanism has an important translation aspect. As ferroptosis is a reasonably new described type of cell death, there are numerous mechanisms that still need to be investigated. In this thesis we provide initial characterization on the role of a specific intermediate of the cholesterol biosynthetic pathway, namely 7-DHC, on ferroptosis. Based on the fact that lipid peroxidation assumes a central role for ferroptosis, sterol metabolism is a useful target point for research on compounds sensitizing to this form of cell death. To emphasize the extensive meaning of 7-DHC, some exemplary processes are mentioned hereafter, which we believe based on our results could catalyze further research.

Cholesterol has a large variety of biological functions and due to its complex biosynthetic pathway, defects in their formation, not surprisingly, have been associated to several diseases. The Smith-Lemi-Opitz Syndrome (SLOS) is the first human disease discovered that is based on a congenital defective sterol synthesis [90]. It results from mutations in DHCR7, the enzyme synthesizing cholesterol and leads to increased levels of 7-DHC and its isomer 8-DHC [91]. The responsible enzyme is defined but the role of the metabolites and mechanisms involved in the pathology of SLOS still need to be studied in more detail. 7-DHC is highly oxidizable, circa 200 times more reactive than cholesterol concerning free radical chain oxidation [92]. Oxysterols derived from 7-DHC and metabolites of 7-DHC and 8-DHC have been demonstrated to be cytotoxic [93]. Our results conversely show that DHCR7 deficiency resulting in increased 7-DHC levels has a cell protective effect. This underscored our incomplete understanding on the mechanism involved on 7-DHC and its metabolites. Our experiments rely on the assumption that DHCR7 dysfunction leads to an increased level of 7-DHC but there might be more metabolites, especially oxidation products, which result from DHCR7 deficiency and are involved in the pathology of SLOS. Concerning our experiments, it is necessary to further assess the formation of oxysterol products. Cytotoxic effects of 7-DHC have been associated to different mechanisms. In lymphocytes of SLOS patients the altered sterol composition was shown to inhibit the function of voltage-gated Kv1.3 channels controlling T cell function. The sensitivity of Kv1.3 channels was assessed by treating the

cells with the same concentration of 7-DHC and cholesterol. The average activation time constant of Kv1.3 was significantly extended by 7-DHC but not by cholesterol at a concentration of 32.5 µM [94]. In melanoma cells, increased production of reactive oxygen species, increase in apoptosis-inducing factor levels (e.g. Bax), reduction of mitochondrial membrane potential and absence of PARP-1 cleavage were established [95]. Gelzo and Granato et al. compared two concentrations of 7-DHC, 19.2 µg/ml and 38.5 µg/ml in their experiments, whereby the cell-damaging and pro-apoptotic effects are reinforced when using the higher 7-DHC concentration. A research group of Korade et al. identified several oxysterols formed from oxidation of 7-DHC that reduce cell viability in a dose dependent manner (**Figure 21**). They were also able to show that cytotoxicity of oxysterols is related to their nucleus structure whereas a reduced 7-DHC oxysterol mixture is more toxic and significantly reduces cell viability already at a concentration of 10 µM. Different oxysterol mixture concentrations up to 50 µM were compared [93]. For our experiments, that revealed a protective effect of 7-DHC, we added up to only 10 µM of exogenous 7-DHC (**Figure 11A**, **Figure 12B**, **Figure 18**), more over it has to be stated that concentrations higher than 20µM for any of the given sterol crystallization and precipitation was noticed. Therefore, in the previous studies it is difficult to establish if the effects are due to the sterols or the formed crystals. Thus, with regard to a potential pharmacological application of 7-DHC the concentration plays a decisive role for its function.

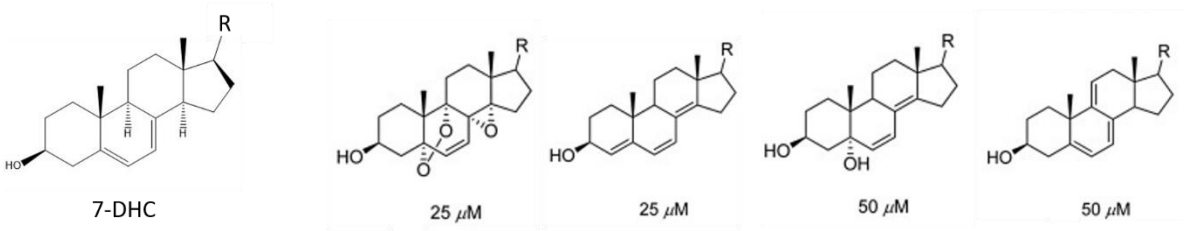

Figure 21. 7-DHC oxysterols *Structural formula of oxysterols derived from 7-DHC. The concentration below each compound shows the oxysterol concentration that leads to reduction in cell survival to ≤50%, 48 h after the treatment. Chemical structures adapted from Korade, Xu, Shelton and Porter [93].*

4.1 Antipsychotics drugs,7-DHC level and teratogenicity

It is not only essential for the comprehension of SLOS to understand all mechanisms of DHCR7 deficiency. Ariprazole (ARI) and trazodone (TRZ) are common and widespread antipsychotics that target DHCR7. Treatment with ARI and TRZ leads to increased plasma levels of 7-DHC, which can ultimately lead to a misdiagnosis as SLOS patients [96]. SLOS is a recessive disease with a heterozygous carrier frequency of 1-3 % [97]. Korade et al. revealed that heterozygous DHCR7$^{+/-}$ carriers are more vulnerable to ARI and TRZ exposure and to their deleterious impact on sterol homeostasis. The authors have reported that exposure to DHCR7 inhibitors during pregnancy has teratogenic effect, this is particularly relevant given that 1-3 % of the population are heterozygous carriers for DHCR7 mutations. It also needs to be considered that apart from ARI and TRZ, there are several other pharmaceuticals affecting the 7-DHC level in Neuro2a cells [98], [99]. In line with these results, one could be provocative to consider that, just like defects in apoptotic cell death leading to embryonic malformations, it is possible that malformations of SLOS patients can be traced to lack of ferroptosis due to increased 7-DHC levels. Potentially underscoring and important relevant function for ferroptosis as a programed cell death modality.

4.2 Hepatitis B virus and 7-DHC

Viruses are pathogenic agents that co-opt host metabolism for successful replication and assembling. Especially cellular lipids as membrane components are essential for virus replication. Cholesterol has been demonstrated to be essential for the replication of several viruses, such as herpes simplex [100], influenza [101], vaccinia [102] and Epstein-Barr [103]. Curiously, a correlation between 7-DHC and human hepatitis B virus (HBV) has been proposed. Using liquid chromatography-mass spectrometry (LC-MS) Rodgers et al. were able to detect a selective abundance of 7-DHC in cells replicating HBV. Therefore, it remains to be shown if 7-DHC accumulation supports viral replication by means, such as suppressing ferroptosis. As viral infections are associated with changes in lipid metabolism, sterols may provide important pharmacological actionable nodes as therapeutic targets to control virus replication [104]. The correlation between HBV infection and the increased accumulation of 7-DHC emphasizes the importance of more in-depth research on DHCR7 function and the biology of 7-DHC.

5 Abstract

Cell death is an essential aspect of life that plays an important role for successful development and tissue remodeling as well as for diseases. There are several different types of cell death that differ from each other in morphological, functional and biochemical ways. Regulated cell death that occurs in physiological processes is generally equated with programmed cell death (PCD), whereby apoptosis is the most studied form of PCD. Ferroptosis is a form of regulated cell death and unique in its requirements for iron and lipid peroxidation. It is linked to numerous biological processes, such as amino acid metabolism, phospholipid metabolism and sterol synthesis. Cholesterol biosynthesis is a complex pathway with a large number of enzymes and substrates that are potential target points for cellular dysfunctions. Motivated by the results from a CRISPR-based genetic screening in this thesis, we focused on 7-dehydrocholesterol reductase (DHCR7), the enzyme responsible for conversion of 7-dehydrocholesterol (7-DHC) to cholesterol. In this work we focused on the ferroptosis sensitive cell line HT1080 and generated a series of models to address the importance of DHCR7 in ferroptosis. Using CRISPR/Cas9, HT1080 DHCR7_KO and DHCR7/SC5D_KO cell lines were generated and used to validate their sensitivity against ferroptosis inducers and sterol consumption. We could show that 7-DHC is a strong antiferroptotic agent that could prevent cell death in genetic models as well as when supplemented directly to cells. Importantly, all the results obtained were subsequently confirmed in isogenic reconstituted pairs from the HT1080 DHCR7/SC5D_KO. Moreover, we demonstrate that this protective effect is not due to an inherent and unspecific resistance as the sensitivity to non-ferroptotic stimuli was equally effective in killing the HT1080 DHCR7_KO and DHCR7/SC5D_KO cell lines. We could also show that selenium present in the media has a strong impact on the activity of 7-DHC and this is because in its absence the effective concentration is rapidly decreased. Surprisingly we also demonstrate that removing sterol from cell culture triggers ferroptosis in cells unable to synthesize 7-DHC, suggestive that this could be used as a novel mechanism to trigger ferroptosis. Ultimately, in the present work we could show that unlike previously reported, 7-DHC is not only a toxic intermediate of the cholesterol biosynthesis pathway but under specific circumstances it has a strong pro-survival effect.

Zusammenfassung

Der Zelltod ist ein unabdingbarer Bestandteil des Lebens, der sowohl für gesunde Entwicklung und Gewebeumbau, als auch für Krankheiten eine wichtige Rolle spielt. Es gibt viele verschiedene Arten des Zelltods, die sich in morphologischer, funktioneller und biochemischer Hinsicht unterscheiden. Regulierter Zelltod tritt im Rahmen physiologischer Prozesse auf und wird allgemein mit dem programmierten Zelltod gleichgesetzt, zu dem auch die am meisten untersuchte Apoptose gehört. Die von uns untersuchte Ferroptose ist eine Form des regulierten Zelltodes und einzigartig in ihrem Bedarf an Eisen und Lipidperoxidation. Sie ist mit zahlreichen biologischen Prozessen verknüpft, wie z.B. dem Aminosäuren- und Phospholipidstoffwechsel und der Sterolsynthese. Die Cholesterinbiosynthese ist ein komplexer Weg mit einer Vielzahl an Enzymen und Substraten, die potentielle Angriffspunkte für zelluläre Funktionsstörungen darstellen. Motiviert durch die Ergebnisse eines CRISPR-basierten genetischen Screenings haben wir uns in dieser Arbeit auf die 7-Dehydrocholesterol-Reduktase (DHCR7) konzentriert, das Enzym, das für die Umwandlung von 7-Dehydrocholesterol (7-DHC) in Cholesterol verantwortlich ist. In dieser Arbeit konzentrierten wir uns auf die ferroptosesensitive Zelllinie HT1080 und erstellten eine Reihe von Modellen, um die Bedeutung von DHCR7 in der Ferroptose zu untersuchen. Mittels CRISPR/Cas9 wurden HT1080 DHCR7_KO und DHCR7/SC5D_KO Zelllinien generiert und ihre Sensitivität gegenüber Ferroptose-Induktoren und ihr Sterolverbrauch validiert. Wir konnten zeigen, dass 7-DHC eine starke antiferroptotische Verbindung ist, die sowohl in genetischen Modellen als auch bei direkter Zugabe den Zelltod verhindern kann. Hervorzuheben ist, dass alle erhaltenen Ergebnisse anschließend anhand isogen rekonstituierter Paare aus den HT1080 DHCR7/SC5D_KO Zellen bestätigt wurden. Darüber hinaus wird gezeigt, dass dieses protektive Mittel nicht auf eine inhärente und unspezifische Resistenz zurückzuführen ist, da die Empfindlichkeit gegenüber nicht-ferroptotischen Stimuli gleichermaßen effektiv bei der Abtötung der Zelllinien HT1080 DHCR7_KO und DHCR7/SC5D_KO war. Wir konnten auch zeigen, dass in den Zellmedien vorhandenes Selen einen starken Einfluss auf die Aktivität von 7-DHC hat, da in Abwesenheit von Selen die effektive Konzentration schnell abnimmt. Überraschenderweise konnten wir auch feststellen, dass die Entfernung von Sterolen aus dem

Nährmedium Ferroptose in Zellen auslöst, die nicht in der Lage sind, 7-DHC zu synthetisieren. Dies regt dazu an, dass dieser Mechanismus zur Auslösung von Ferroptose genutzt werden könnte. Letztendlich konnten wir in der vorliegenden Arbeit darlegen, dass 7-DHC im Gegensatz zu den bisherigen Berichten nicht nur ein toxisches Zwischenprodukt der Cholesterinbiosynthese ist, sondern unter bestimmten Umständen eine starke überlebensfördernde Wirkung hat.

6 References

1. Kagan, V.E. *et al*. Oxidized arachidonic and adrenic PEs navigate cells to ferroptosis. *Nat Chem Biol* **13**, 81-90 (2017).
2. Galluzzi, L. *et al*. Molecular mechanisms of cell death: recommendations of the Nomenclature Committee on Cell Death 2018. *Cell Death Differ* **25**, 486-541 (2018).
3. Perez-Garijo, A. & Steller, H. Spreading the word: non-autonomous effects of apoptosis during development, regeneration and disease. *Development* **142**, 3253-3262 (2015).
4. Schaefer, L. Complexity of danger: the diverse nature of damage-associated molecular patterns. *The Journal of biological chemistry* **289**, 35237-35245 (2014).
5. Bergmann, A. & Steller, H. Apoptosis, stem cells, and tissue regeneration. *Science signaling* **3**, re8 (2010).
6. Stephen W. G. Tait, G.I.a.D.R.G. Die another way – non-apoptotic mechanisms of cell death. *Journal of Cell Science* (2014).
7. Tavernarakis, N. & Driscoll, M. Cell/Neuron Degeneration, in *Encyclopedia of Genetics*. (eds. S. Brenner & J.H. Miller) 313-318 (Academic Press, New York; 2001).
8. Lipton, P. Ischemic cell death in brain neurons. *Physiological reviews* **79**, 1431-1568 (1999).
9. Menendez, J., Perez-Garijo, A., Calleja, M. & Morata, G. A tumor-suppressing mechanism in Drosophila involving cell competition and the Hippo pathway. *Proceedings of the National Academy of Sciences of the United States of America* **107**, 14651-14656 (2010).
10. Vogt, K.C. Untersuchungen über die Entwicklungsgeschichte der Geburtshelferkroete (Alytes obstetricans). (1842).
11. Virchow, R. Die Cellularpathologie in ihrer Begründung auf physiologische und pathologische Gewebelehre. 440 (1858).
12. Glücksmann, A. Cell deaths in normal vertebrate ontogeny. **26**, 59-86 (1951).
13. Lockshin, R.A. & Williams, C.M. Programmed cell death. IV. The influence of drugs on the breakdown of the intersegmental muscles of silkmoths. *Journal of insect physiology* **11**, 803-809 (1965).
14. Kerr, J.F., Wyllie, A.H. & Currie, A.R. Apoptosis: a basic biological phenomenon with wide-ranging implications in tissue kinetics. *British journal of cancer* **26**, 239-257 (1972).
15. Schweichel, J.U. & Merker, H.-J. *The morphology of various types of cell death in prenatal tissues*, Vol. 7. (1973).
16. Arvanitis, M., Li, D.-D., Lee, K. & Mylonakis, E. Apoptosis in C. elegans: lessons for cancer and immunity. *Frontiers in cellular and infection microbiology* **3**, 67-67 (2013).
17. Gartner, A., Boag, P.R. & Blackwell, T.K. Germline survival and apoptosis. *WormBook : the online review of C. elegans biology*, 1-20 (2008).
18. Potten, C.S. Extreme sensitivity of some intestinal crypt cells to X and γ irradiation. *Nature* **269**, 518-521 (1977).

19. Wyllie, A.H. Glucocorticoid-induced thymocyte apoptosis is associated with endogenous endonuclease activation. *Nature* **284**, 555-556 (1980).
20. Jeffrey Hall, J.D., Theodore Friedmann, Francesco Giannelli *Advances in Genetics, Volume 35*. (1997).
21. Zhang, D.W. *et al.* RIP3, an energy metabolism regulator that switches TNF-induced cell death from apoptosis to necrosis. *Science (New York, N.Y.)* **325**, 332-336 (2009).
22. Fuchs, Y. & Steller, H. Programmed cell death in animal development and disease. *Cell* **147**, 742-758 (2011).
23. Durand, P.M. & Ramsey, G.J.B.T. The Nature of Programmed Cell Death. **14**, 30-41 (2019).
24. D'Arcy, M.S. Cell death: a review of the major forms of apoptosis, necrosis and autophagy. **43**, 582-592 (2019).
25. Chen, Q., Kang, J. & Fu, C. The independence of and associations among apoptosis, autophagy, and necrosis. *Signal Transduction and Targeted Therapy* **3**, 18 (2018).
26. Lavrik, I., Golks, A. & Krammer, P.H. Death receptor signaling. *J Cell Sci* **118**, 265-267 (2005).
27. Wang, Y. & Tjandra, N. Structural insights of tBid, the caspase-8-activated Bid, and its BH3 domain. *J Biol Chem* **288**, 35840-35851 (2013).
28. Niemann, B. & Rohrbach, S. Chapter 3 - Metabolically Relevant Cell Biology – Role of Intracellular Organelles for Cardiac Metabolism, in *The Scientist's Guide to Cardiac Metabolism*. (eds. M. Schwarzer & T. Doenst) 19-38 (Academic Press, Boston; 2016).
29. Moriwaki, K. & Chan, F.K. RIP3: a molecular switch for necrosis and inflammation. *Genes Dev* **27**, 1640-1649 (2013).
30. Murphy, J.M. *et al.* The pseudokinase MLKL mediates necroptosis via a molecular switch mechanism. *Immunity* **39**, 443-453 (2013).
31. Cai, Z. *et al.* Plasma membrane translocation of trimerized MLKL protein is required for TNF-induced necroptosis. *Nature cell biology* **16**, 55-65 (2014).
32. Jorgensen, I. & Miao, E.A. Pyroptotic cell death defends against intracellular pathogens. *Immunological reviews* **265**, 130-142 (2015).
33. Liu, X. *et al.* Inflammasome-activated gasdermin D causes pyroptosis by forming membrane pores. *Nature* **535**, 153 (2016).
34. Henao-Mejia, J., Elinav, E., Strowig, T. & Flavell, R.A. Inflammasomes: far beyond inflammation. *Nature immunology* **13**, 321-324 (2012).
35. Wang, Y. *et al.* A nuclease that mediates cell death induced by DNA damage and poly(ADP-ribose) polymerase-1. *Science (New York, N.Y.)* **354** (2016).
36. Doll, S. *et al.* ACSL4 dictates ferroptosis sensitivity by shaping cellular lipid composition. *Nature Chemical Biology* **13**, 91 (2016).
37. Stockwell, B.R. *et al.* Ferroptosis: A Regulated Cell Death Nexus Linking Metabolism, Redox Biology, and Disease. *Cell* **171**, 273-285 (2017).
38. Griffith, O.W. & Meister, A. Potent and specific inhibition of glutathione synthesis by buthionine sulfoximine (S-n-butyl homocysteine sulfoximine). *J Biol Chem* **254**, 7558-7560 (1979).
39. Yang, W.S. *et al.* Regulation of ferroptotic cancer cell death by GPX4. *Cell* **156**, 317-331 (2014).

40. Yagoda, N. *et al.* RAS–RAF–MEK-dependent oxidative cell death involving voltage-dependent anion channels. *Nature* **447**, 865 (2007).
41. Friedmann Angeli, J.P. *et al.* Inactivation of the ferroptosis regulator Gpx4 triggers acute renal failure in mice. *Nature cell biology* **16**, 1180-1191 (2014).
42. Yang, W.S. & Stockwell, B.R. Synthetic lethal screening identifies compounds activating iron-dependent, nonapoptotic cell death in oncogenic-RAS-harboring cancer cells. *Chemistry & biology* **15**, 234-245 (2008).
43. Dixon, S.J. & Stockwell, B.R. The role of iron and reactive oxygen species in cell death. *Nature Chemical Biology* **10**, 9 (2013).
44. Fang, X. *et al.* Ferroptosis as a target for protection against cardiomyopathy. **116**, 2672-2680 (2019).
45. Forcina, G.C. & Dixon, S.J. GPX4 at the Crossroads of Lipid Homeostasis and Ferroptosis. **0**, 1800311 (2019).
46. Liu, H., Schreiber, S.L. & Stockwell, B.R. Targeting Dependency on the GPX4 Lipid Peroxide Repair Pathway for Cancer Therapy. *Biochemistry* **57**, 2059-2060 (2018).
47. Dixon, S.J. *et al.* Human Haploid Cell Genetics Reveals Roles for Lipid Metabolism Genes in Nonapoptotic Cell Death. *ACS Chemical Biology* **10**, 1604-1609 (2015).
48. Zilka, O. *et al.* On the Mechanism of Cytoprotection by Ferrostatin-1 and Liproxstatin-1 and the Role of Lipid Peroxidation in Ferroptotic Cell Death. *ACS Central Science* **3**, 232-243 (2017).
49. Skouta, R. *et al.* Ferrostatins inhibit oxidative lipid damage and cell death in diverse disease models. *J Am Chem Soc* **136**, 4551-4556 (2014).
50. Buhaescu, I. & Izzedine, H. Mevalonate pathway: A review of clinical and therapeutical implications. *Clinical Biochemistry* **40**, 575-584 (2007).
51. Warner, G.J. *et al.* Inhibition of selenoprotein synthesis by selenocysteine tRNA[Ser]Sec lacking isopentenyladenosine. *J Biol Chem* **275**, 28110-28119 (2000).
52. Viswanathan, V.S. *et al.* Dependency of a therapy-resistant state of cancer cells on a lipid peroxidase pathway. *Nature* **547**, 453-457 (2017).
53. Garcia-Bermudez, J. *et al.* Squalene accumulation in cholesterol auxotrophic lymphomas prevents oxidative cell death. *Nature* **567**, 118-122 (2019).
54. Shimada, K. *et al.* Global survey of cell death mechanisms reveals metabolic regulation of ferroptosis. *Nat Chem Biol* **12**, 497-503 (2016).
55. Madison, B.B. Srebp2: A master regulator of sterol and fatty acid synthesis. *Journal of lipid research* **57**, 333-335 (2016).
56. Shimano, H. & Sato, R. SREBP-regulated lipid metabolism: convergent physiology — divergent pathophysiology. *Nature Reviews Endocrinology* **13**, 710 (2017).
57. Vergnes, L. *et al.* SREBP-2-deficient and hypomorphic mice reveal roles for SREBP-2 in embryonic development and SREBP-1c expression. *Journal of lipid research* **57**, 410-421 (2016).
58. Brown, M.S. & Goldstein, J.L. A proteolytic pathway that controls the cholesterol content of membranes, cells, and blood. *Proceedings of the National Academy of Sciences of the United States of America* **96**, 11041-11048 (1999).
59. Addison, James & Jennifer Biology and Applications of CRISPR Systems: Harnessing Nature's Toolbox for Genome Engineering. *Cell* **164**, 29-44 (2016).

60. Mojica, F.J.M., Díez-Villaseñor, C., Almendros, C. & García-Martínez, J. Short motif sequences determine the targets of the prokaryotic CRISPR defence system. *Microbiology* **155**, 733-740 (2009).
61. Datsenko, K.A. *et al.* Molecular memory of prior infections activates the CRISPR/Cas adaptive bacterial immunity system. *Nature Communications* **3**, 945 (2012).
62. Deltcheva, E. *et al.* CRISPR RNA maturation by trans-encoded small RNA and host factor RNase III. *Nature* **471**, 602-607 (2011).
63. Gasiunas, G., Barrangou, R., Horvath, P. & Siksnys, V. Cas9-crRNA ribonucleoprotein complex mediates specific DNA cleavage for adaptive immunity in bacteria. *Proceedings of the National Academy of Sciences* **109**, E2579-E2586 (2012).
64. Samuel & Jennifer Expanding the Biologist's Toolkit with CRISPR-Cas9. *Molecular Cell* **58**, 568-574 (2015).
65. Wang, T., Wei, J.J., Sabatini, D.M. & Lander, E.S. Genetic screens in human cells using the CRISPR-Cas9 system. *Science (New York, N.Y.)* **343**, 80-84 (2014).
66. Cong, L. *et al.* Multiplex genome engineering using CRISPR/Cas systems. *Science (New York, N.Y.)* **339**, 819-823 (2013).
67. Shalem, O. *et al.* Genome-scale CRISPR-Cas9 knockout screening in human cells. *Science (New York, N.Y.)* **343**, 84-87 (2014).
68. Tzelepis, K. *et al.* A CRISPR Dropout Screen Identifies Genetic Vulnerabilities and Therapeutic Targets in Acute Myeloid Leukemia. *Cell reports* **17**, 1193-1205 (2016).
69. Porter, J.A., Young, K.E. & Beachy, P.A. Cholesterol modification of hedgehog signaling proteins in animal development. *Science (New York, N.Y.)* **274**, 255-259 (1996).
70. Huff, T. & Jialal, I. Physiology, Cholesterol, in *StatPearls* (Treasure Island (FL); 2019).
71. Nes, W.D. Biosynthesis of cholesterol and other sterols. *Chem Rev* **111**, 6423-6451 (2011).
72. Herman, G.E. Disorders of cholesterol biosynthesis: prototypic metabolic malformation syndromes. *Human molecular genetics* **12 Spec No 1**, R75-88 (2003).
73. Kempen, H.J., Glatz, J.F., Gevers Leuven, J.A., van der Voort, H.A. & Katan, M.B. Serum lathosterol concentration is an indicator of whole-body cholesterol synthesis in humans. *Journal of lipid research* **29**, 1149-1155 (1988).
74. Xu, L., Liu, W., Sheflin, L.G., Fliesler, S.J. & Porter, N.A. Novel oxysterols observed in tissues and fluids of AY9944-treated rats: a model for Smith-Lemli-Opitz syndrome. *Journal of lipid research* **52**, 1810-1820 (2011).
75. Hatfield, D.L. & Gladyshev, V.N. How selenium has altered our understanding of the genetic code. *Mol Cell Biol* **22**, 3565-3576 (2002).
76. Kryukov, G.V. *et al.* Characterization of Mammalian Selenoproteomes. *Science (New York, N.Y.)* **300**, 1439-1443 (2003).
77. Ursini, F., Maiorino, M., Valente, M., Ferri, L. & Gregolin, C. Purification from pig liver of a protein which protects liposomes and biomembranes from peroxidative degradation and exhibits glutathione peroxidase activity on phosphatidylcholine

hydroperoxides. *Biochimica et Biophysica Acta (BBA) - Lipids and Lipid Metabolism* **710**, 197-211 (1982).
78. Prelich, G. Gene overexpression: uses, mechanisms, and interpretation. *Genetics* **190**, 841-854 (2012).
79. Horlick, L. Effect of a new inhibitor of cholesterol biosynthesis (AY 9944) on serum and tissue sterols in the rat. *Journal of lipid research* **7**, 116-121 (1966).
80. Aufenanger, J., Pill, J., Schmidt, F.H. & Stegmeier, K. The effects of BM 15.766, an inhibitor of 7-dehydrocholesterol δ7-reductase∗, on cholesterol biosynthesis in primary rat hepatocytes. *Biochemical Pharmacology* **35**, 911-916 (1986).
81. Horling, A., Muller, C., Barthel, R., Bracher, F. & Imming, P. A new class of selective and potent 7-dehydrocholesterol reductase inhibitors. *J Med Chem* **55**, 7614-7622 (2012).
82. Linkermann, A. *et al.* Synchronized renal tubular cell death involves ferroptosis. *Proc Natl Acad Sci U S A* **111**, 16836-16841 (2014).
83. Dixon, S.J. *et al.* Ferroptosis: an iron-dependent form of nonapoptotic cell death. *Cell* **149**, 1060-1072 (2012).
84. Chen, D., Frezza, M., Schmitt, S., Kanwar, J. & Dou, Q.P. Bortezomib as the first proteasome inhibitor anticancer drug: current status and future perspectives. *Curr Cancer Drug Targets* **11**, 239-253 (2011).
85. Ziogas, D.C., Terpos, E., Kastritis, E. & Dimopoulos, M.A. An overview of the role of carfilzomib in the treatment of multiple myeloma. *Expert Opin Pharmacother* **18**, 1883-1897 (2017).
86. Harper, M.T. Auranofin, a thioredoxin reductase inhibitor, causes platelet death through calcium overload. *Platelets* **30**, 98-104 (2019).
87. Feil, S., Valtcheva, N. & Feil, R. Inducible Cre Mice. *Methods in molecular biology (Clifton, N.J.)* **530**, 343-363 (2009).
88. Feil, R. *et al.* Ligand-activated site-specific recombination in mice. *Proceedings of the National Academy of Sciences of the United States of America* **93**, 10887-10890 (1996).
89. Seiler, A. *et al.* Glutathione Peroxidase 4 Senses and Translates Oxidative Stress into 12/15-Lipoxygenase Dependent- and AIF-Mediated Cell Death. *Cell Metabolism* **8**, 237-248 (2008).
90. Irons, M., Elias, E.R., Salen, G., Tint, G.S. & Batta, A.K. Defective cholesterol biosynthesis in Smith-Lemli-Opitz syndrome. *Lancet* **341**, 1414 (1993).
91. Batta, A.K., Tint, G.S., Shefer, S., Abuelo, D. & Salen, G. Identification of 8-dehydrocholesterol (cholesta-5,8-dien-3 beta-ol) in patients with Smith-Lemli-Opitz syndrome. *Journal of lipid research* **36**, 705-713 (1995).
92. Xu, L., Korade, Z. & Porter, N.A. Oxysterols from free radical chain oxidation of 7-dehydrocholesterol: product and mechanistic studies. *J Am Chem Soc* **132**, 2222-2232 (2010).
93. Korade, Z., Xu, L., Shelton, R. & Porter, N.A. Biological activities of 7-dehydrocholesterol-derived oxysterols: implications for Smith-Lemli-Opitz syndrome. *Journal of lipid research* **51**, 3259-3269 (2010).

94. Balajthy, A. *et al.* 7DHC-induced changes of Kv1.3 operation contributes to modified T cell function in Smith-Lemli-Opitz syndrome. *Pflügers Archiv - European Journal of Physiology* **468**, 1403-1418 (2016).
95. Gelzo, M. *et al.* Evaluation of cytotoxic effects of 7-dehydrocholesterol on melanoma cells. *Free Radic Biol Med* **70**, 129-140 (2014).
96. Korade, Z. *et al.* Effect of psychotropic drug treatment on sterol metabolism. *Schizophr Res* **187**, 74-81 (2017).
97. Cross, J.L. *et al.* Determination of the allelic frequency in Smith-Lemli-Opitz syndrome by analysis of massively parallel sequencing data sets. *Clin Genet* **87**, 570-575 (2015).
98. Boland, M.R. & Tatonetti, N.P. Investigation of 7-dehydrocholesterol reductase pathway to elucidate off-target prenatal effects of pharmaceuticals: a systematic review. *Pharmacogenomics J* **16**, 411-429 (2016).
99. Kim, H.Y. *et al.* Inhibitors of 7-Dehydrocholesterol Reductase: Screening of a Collection of Pharmacologically Active Compounds in Neuro2a Cells. *Chem Res Toxicol* **29**, 892-900 (2016).
100. Itzhaki, R.F. & Wozniak, M.A. Herpes simplex virus type 1, apolipoprotein E, and cholesterol: a dangerous liaison in Alzheimer's disease and other disorders. *Prog Lipid Res* **45**, 73-90 (2006).
101. Sun, X. & Whittaker, G.R. Role for influenza virus envelope cholesterol in virus entry and infection. *J Virol* **77**, 12543-12551 (2003).
102. Chung, C.S., Huang, C.Y. & Chang, W. Vaccinia virus penetration requires cholesterol and results in specific viral envelope proteins associated with lipid rafts. *J Virol* **79**, 1623-1634 (2005).
103. Katzman, R.B. & Longnecker, R. Cholesterol-dependent infection of Burkitt's lymphoma cell lines by Epstein-Barr virus. *J Gen Virol* **84**, 2987-2992 (2003).
104. Rodgers, M.A., Saghatelian, A. & Yang, P.L. Identification of an overabundant cholesterol precursor in hepatitis B virus replicating cells by untargeted lipid metabolite profiling. *J Am Chem Soc* **131**, 5030-5031 (2009).

List of figures

Figure 1. Intrinsic and extrinsic apoptosis signaling pathways 4
Figure 2. TNFR signaling pathways 6
Figure 3. Ferroptosis modulating events 8
Figure 4. Cholesterol biosynthesis 12
Figure 5. SREBPs regulating lipid homeostasis 14
Figure 6. CRISPR Cas9 system 16
Figure 7. Vector map 23
Figure 8. Identification of DHCR7 as a new pro-ferroptotic gene 37
Figure 9. Structural formula of 7-Dehydrocholesterol and Cholesterol 38
Figure 10. DHCR7 and SC5D deficiency 39
Figure 11. Sterol effect on DHCR7 and SC5D deficiency 41
Figure 12. Selenium impact 43
Figure 13. Cell generation 44
Figure 14. Re-expression of DHCR7 and SC5D in HT1080 DHCR7/SC5D_KO cells 45
Figure 15. Selenium affects re-expression of DHCR7 and SC5D 47
Figure 16. Pharmacological inhibition of DHCR7 48
Figure 17. Compound sensitivity 50
Figure 18. Impact on different cell lines 51
Figure 19. Genetic model of GPX4 deficiency 53
Figure 20. Impact of delipidated medium 55
Figure 21. 7-DHC oxysterols 57

List of tables

Table 1 List of generated knockouts 30

Appendix

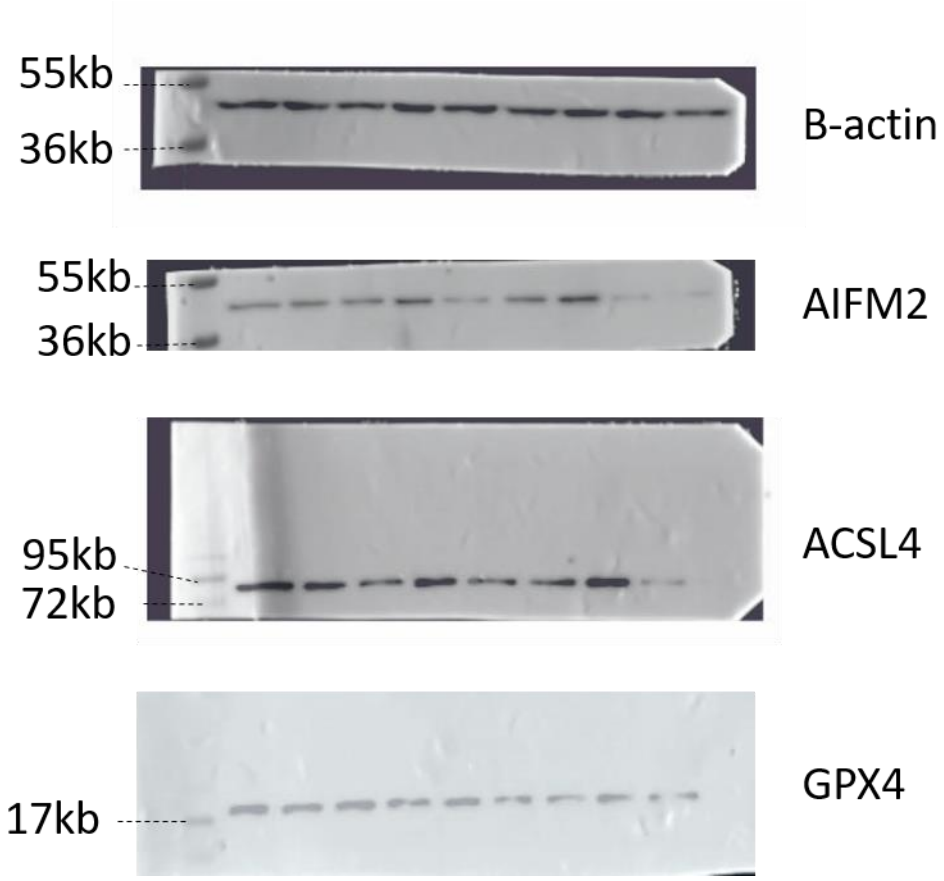

Suppl. figure 1 ***Uncropped western blots of Figure 11***

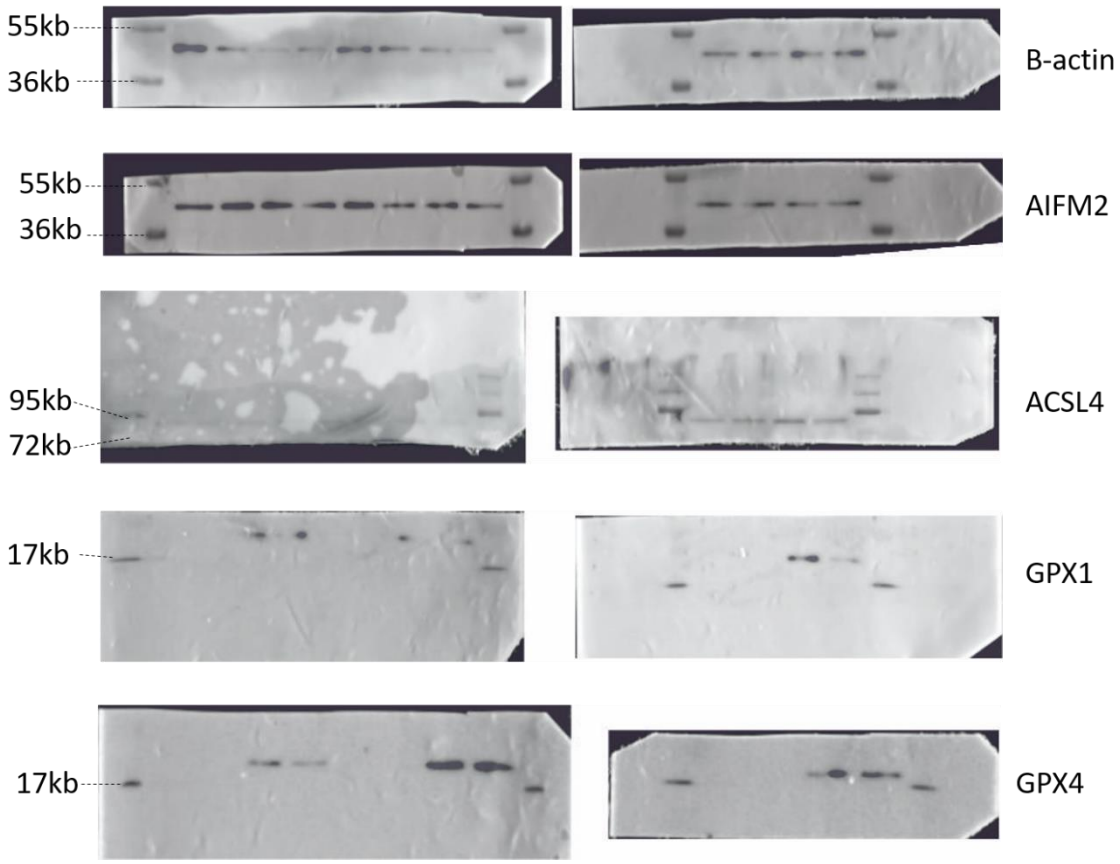

Suppl. figure 2 ***Uncropped western blots of Figure 12***

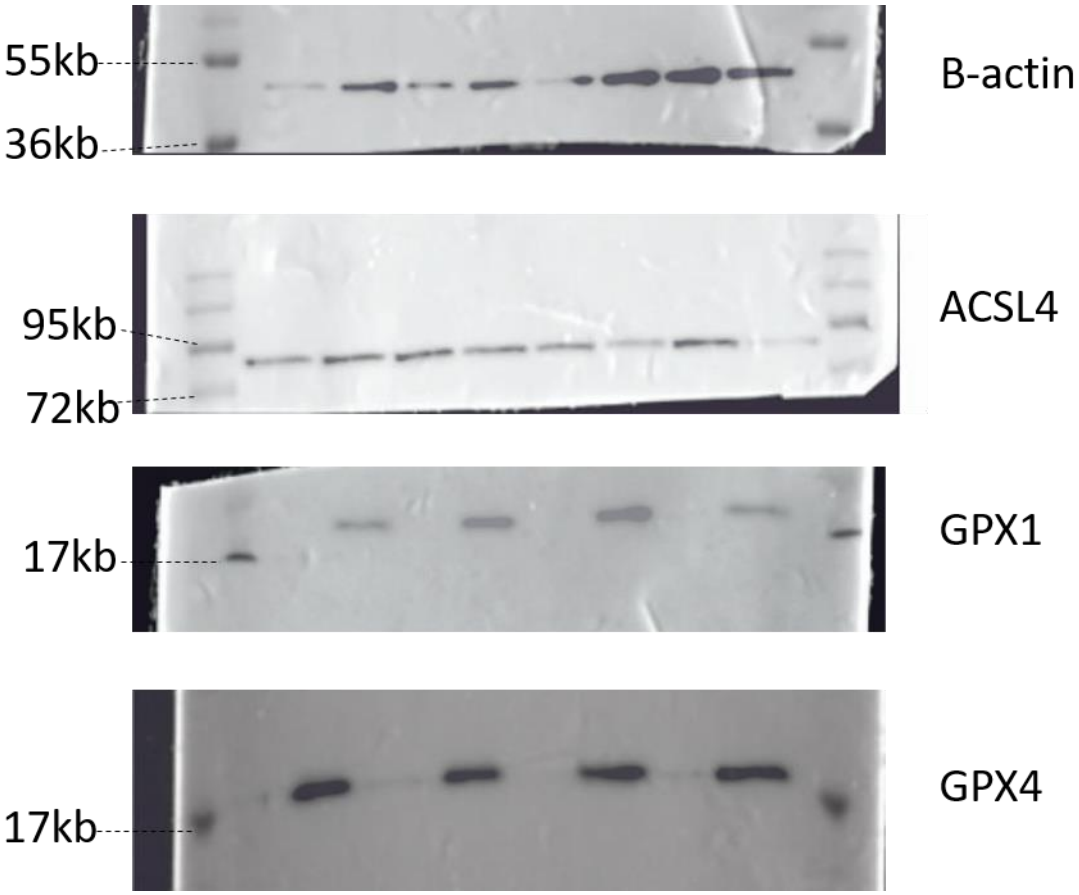

Suppl. figure 3 ***Uncropped western blots of Figure 15***

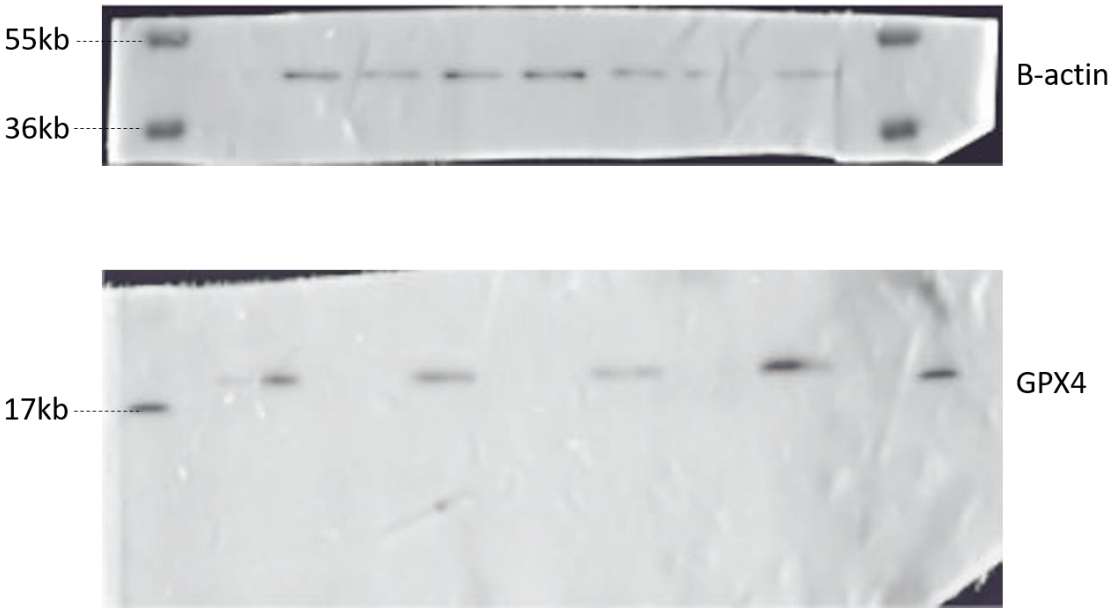

Suppl. figure 4 ***Uncropped western blots of Figure 19***

Acknowledgements

First, I would like to express my sincere gratitude to my supervisor Dr. José Pedro Friedmann Angeli for making my thesis realizable. Thank you for giving me the opportunity to work on this study and providing me the lab facilities. I appreciate his patience, his continuous support, all the motivation and the extraordinary knowledge I gained from him constantly while working on my thesis.

Besides my supervisor, I would like to thank the rest of my thesis committee. Thank you to Prof. Dr. Svenja Meierjohann for making this thesis possible and thank you to Dr. Hans Maric for completing the committee.

A special thank you to my lab mates who made every single day in the lab enjoyable. Thank you for always helping me out and all the fun we had. Thank you to Anne Haberberger to introduce me the daily lab techniques. Thank you to Dr. Florêncio Porto-Freitas for working together with me on the project and for the perfect guiding through all questions. Big thanks also to Thamara Nishida Xavier da Silva who always offers advice and support for all issues, thank you for the encouragement, for all the coffee breaks and being a great friend.

I also would like to thank Dr. Werner Schmitz for providing me his lab facilities and performing the LC/MS analysis of my samples.

Last, I would like to thank my friends and family for being with me all the way through. Thank you for all the ongoing motivation and encouragement and never giving up on me.

Curriculum Vitae

HELENE NEHRING

Nationality: German

Education

01/2019 - 12/2019	Doctoral studies at the Rudolf-Virchow-Zentrum of the University of Würzburg
2013 - 2019	Dental studies at the University of Würzburg Graduation: Staatsexamen
2004 - 2012	Johannes-Gutenberg-Gymnasium Waldkirchen Graduation: Abitur
2000 – 2004	Grundschule St. Marien Lügde

Würzburg, 25.11.2020

_____

Helene Nehring